The following publication J. Zhan, W. -M. Tam and F. C. M. Lau, "Novel Double Protograph LDPC Codes for Joint Source-Channel Coding Systems," in IEEE Transactions on Vehicular Technology, vol. 74, no. 4, pp. 5291-5306, April 2025 is available at https://doi.org/10.1109/TVT.2024.3507919.

# Novel Double Protograph LDPC Codes for Joint Source-Channel Coding Systems

Jia Zhan, Wai-Man Tam, and Francis C. M. Lau Fellow, IEEE

Abstract—In this paper, we first propose a novel joint sourcechannel block code (JSC-BC) in which two protograph-based low-density parity-check (P-LDPC) block codes are connected not only by a source-variable-channel-check (SVCC) linking matrix, but also by a source-check-channel-variable (SCCV) linking matrix that consists of a zero matrix and a lower or upper triangular (base) matrix with "1"s on its diagonal. Also, we simplify the traditional joint protograph extrinsic information transfer (JP-EXIT) algorithm and propose an "untransmitted protographbased EXIT (UP-EXIT) algorithm" for calculating the source threshold of a JSC-BC. The proposed UP-EXIT algorithm is more efficient because a smaller protograph consisting of only the untransmitted VNs (i.e., the source VNs and the punctured channel VNs) and their connected check nodes need to be considered. By using the UP-EXIT algorithm, we search for candidate codes with high source thresholds. Then, we select those among the candidate codes also with low channel thresholds. Theoretical and simulation results show that the newly constructed codes outperform state-of-the-art double P-LDPC (DP-LDPC) block codes. Furthermore, we spatially couple the joint source-channel block code and obtain a spatially coupled joint source-channel code (SC-JSCC). Theoretical analyses and simulation results show that even with a smaller window size and lower decoding complexity, the SC-JSCC with the spatially coupled structure for each sub-block (source protomatrix, channel protomatrix, SCCV linking matrix, and SVCC linking matrix) can achieve better error performance than existing spatially-coupled DP-LDPC codes.

Index Terms—Joint source-channel block code, joint source-channel code (JSCC), SC-DP-LDPC, SC-JSCC, spatially coupled SVCC

#### I. INTRODUCTION

Compared with separated source coding and channel coding, joint source-channel coding in which source and channel encoding/decoding can be performed simultaneously in the same module can achieve lower transmission latency and hardware implementation complexity. Joint source-channel coding utilizes source statistics and channel information to optimize the overall performance, and the technology can be applied to image transmission [1] and video transmission [2].

Various joint source-channel coding schemes have been proposed. In [3], a typical image source coder, namely discrete

Copyright (c) 20xx IEEE. Personal use of this material is permitted. However, permission to use this material for any other purposes must be obtained from the IEEE by sending a request to pubs-permissions@ieee.org.

Jia Zhan was with the Department of Electrical and Electronic Engineering, The Hong Kong Polytechnic University, Hong Kong SAR, China. She is now with Guangdong University of Technology, Guangzhou, China (e-mail: jia1206.zhan@connect.polyu.hk).

Wai-Man Tam and Francis C. M. Lau (corresponding author) are with the Department of Electrical and Electronic Engineering, The Hong Kong Polytechnic University, Hong Kong SAR, China (e-mail: wm.tam@polyu.edu.hk, francis-cm.lau@polyu.edu.hk).

The work described in this paper was partly supported by a RGC Research Impact Fund from the Hong Kong SAR, China (Project No. R5013-19).

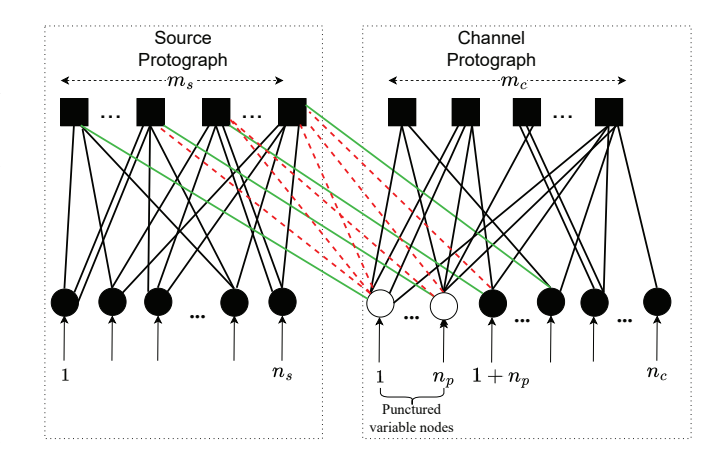


Fig. 1. Protograph representation of DP-LDPC JSCC system.

cosine transform coding, and a convolutional channel code are used in a joint source-channel coding system. Considerable coding gains are achieved by utilizing the image residual redundancy at a priori soft-output Viterbi decoding process. Due to the outstanding error-correction performance of turbo codes [4] and LDPC codes [5], joint source-channel coding systems using them as channel codes together with a source code have been proposed [6], [7]. The source code length in these systems, however, is not fixed. Source codes with variable lengths increase the system implementation complexity and cannot match well with these channel codes with excellent performance. In [8], a concatenated LDPC joint sourcechannel coding scheme is proposed. By using the LDPC code as the source code, a fixed-to-fixed length compressed source sequence is generated. Then, the compressed information is protected by another LDPC code. An iterative source-channel belief propagation (BP) decoding algorithm is used at the receiver and results in good error performance.

Protograph LDPC (P-LDPC) codes [9]–[11], which can be represented by small-size protographs consisting of variable nodes (VNs), check nodes (CNs) and parallel edges, are a sub-class of LDPC codes. They have parallel encoding and decoding structures and the linear minimum Hamming distance property. In [12], double P-LDPC (DP-LDPC) codes replace double randomly constructed LDPC codes in the joint source-channel coding system, forming the DP-LDPC based joint source-channel coding system. The protograph representation of this joint source-channel coding scheme is shown in Fig. 1 with the red dashed lines removed. The source P-LDPC and channel P-LDPC codes are shown in the left dotted frame and the right dotted frame, respectively. Circles and squares, respectively, represent VNs and CNs.

© 2024 IEEE. Personal use of this material is permitted. Permission from IEEE must be obtained for all other uses, in any current or future media, including reprinting/republishing this material for advertising or promotional purposes, creating new collective works, for resale or redistribution to servers or lists, or reuse of any copyrighted component of this work in other works.

In particular, punctured VNs in the channel protograph are represented by blank circles. The green lines connecting CNs in the source protograph and VNs in the channel protograph in a one-to-one manner reflect the cascading relationship between the source encoder and the channel encoder. The protograph shown in Fig. 1 with the red dashed connections removed can be denoted by  $\mathbf{B}_{\mathrm{J}} = \begin{pmatrix} \mathbf{B}_{\mathrm{s}} & \mathbf{B}_{\mathrm{sccv}} \\ \mathbf{0}_{m_c \times n_s} & \mathbf{B}_{\mathrm{c}} \end{pmatrix}$ , where  $\mathbf{B}_{\mathrm{s}}$  of size  $m_s \times n_s$  and  $\mathbf{B}_{\mathrm{c}}$  of size  $m_c \times n_c$  are the source protomatrix and the channel protomatrix, respectively.  $\mathbf{B}_{\mathrm{sccv}}$  of size  $m_s \times n_c$  is the source-check-channel-variable (SCCV) linking protomatrix [13], which consists of a zero matrix  $\mathbf{0}_{m_s \times m_c}$  of size  $m_s \times m_c$  and an identity matrix  $\mathbf{I}_{m_s}$  of size  $m_s \times m_s$ , i.e.,

$$\mathbf{B}_{\text{sccv}} = \begin{pmatrix} \mathbf{I}_{m_s} & \mathbf{0}_{m_s \times m_c} \end{pmatrix}. \tag{1}$$

Various optimization schemes for the DP-LDPC based joint source-channel coding system have been proposed. An unequal error protection (UEP) technique [14] and an unequal power allocation technique [15] are respectively applied in the DP-LDPC based joint source-channel coding system to improve the error performance. In [16], a source protograph extrinsic information transfer (SP-EXIT) algorithm is proposed to calculate the source thresholds of DP-LDPC codes, which provides theoretical guidance for matching source entropy and source encoding rate. In [17], a joint protograph extrinsic information transfer (JP-EXIT) algorithm is proposed for calculating the channel threshold of a DP-LDPC code. (Lower channel thresholds predict better waterfall region performance.) Then, the channel protomatrix  $B_c$  is redesigned based on the JP-EXIT algorithm results to obtain performance improvement. In [18], the source protomatrix  $B_s$  and the channel protomatrix B<sub>c</sub> are redesigned as a code pair to achieve coding gains. The optimal allocation of degree-2 VNs in the joint protomatrix  $B_J$  is studied in [19] and [20]. In [21],  $B_{\rm I}$  is redesigned as a whole and the resulting DP-LDPC codes have excellent error-correction capabilities. In [22], the columns in the identity matrix  $\mathbf{I}_{m_s}$  of  $\mathbf{B}_{\mathrm{sccv}}$  are exchanged to find the optimal connection between VNs in  $\mathbf{B}_c$  and CNs in  $\mathbf{B}_{\mathrm{s}}$  so as to improve the error performance. In [23],  $\mathbf{I}_{m_{\mathrm{s}}}$  in (1) is replaced with a lower or upper triangular sub-base matrix with "1"s on the diagonal. The corresponding SCCV linking matrix can be denoted by

$$\mathbf{B}_{\mathrm{sccv}}^{'} = \begin{pmatrix} \mathbf{T}_{m_s} & \mathbf{0}_{m_s \times m_c} \end{pmatrix}, \tag{2}$$

where  $\mathbf{T}_{m_s}$  denotes the lower or upper triangular protomatrix of size  $m_s \times m_s$  with "1"s on the diagonal. The corresponding DP-LDPC code is denoted by

$$\mathbf{B}_{\mathrm{J}}^{'} = \begin{pmatrix} \mathbf{B}_{\mathrm{s}} & \mathbf{B}_{\mathrm{sccv}}^{'} \\ \mathbf{0}_{m_{c} \times n_{s}} & \mathbf{B}_{\mathrm{c}} \end{pmatrix}. \tag{3}$$

The protograph of  $\mathbf{B}_{\mathrm{J}}'$  is shown in Fig. 1 with both green and red dashed connections forming  $\mathbf{T}_{m_s}$ . It has also been shown that  $\mathbf{B}_{\mathrm{J}}'$  outperforms  $\mathbf{B}_{\mathrm{J}}$ . Later, in [24], a global optimization is used for designing DP-LDPC codes, where the SCCV linking base matrix consists of a zero matrix and a non-identity matrix.

It has been proved in [25], [26] that compared with LDPC block codes, LDPC convolutional codes can obtain convolutional gain by using an iterative BP algorithm. When LDPC convolutional codes are terminated, the corresponding codes are called spatially coupled LDPC (SC-LDPC) codes [27], [28]. In [29], two spatially coupled regular LDPC codes are concatenated by an identity matrix in a joint source-channel coding system, and a sliding window joint source-channel decoder is exploited. These codes are shown to possess better error performance compared with the DP-LDPC block codes used in [17]. Recently, a new type of SC-DP-LDPC code whose SCCV linking matrix has a spatially coupled structure is proposed [30]. Both theoretical and simulation results have demonstrated its superiority over existing DP-LDPC codes.

The joint source-channel coding schemes mentioned above all focus on code optimization for low-entropy sources. There are only a few results for high-entropy sources. In [31], it is shown that error floors caused by the source compression can be lowered by adding connections between VNs in the source LDPC code and CNs in the channel LDPC code. In [32], similar connections, shown as blue connections in Fig. 2, are added in the DP-LDPC codes. The relationship between the newly added connections and the error performance is investigated. In [33], some design rules for the new connections between VNs in the source P-LDPC and CNs in the channel P-LDPC are proposed for both low-entropy and highentropy sources. In [13], the source protograph and the sourcevariable-channel-check (SVCC) linking matrix are designed as a whole to obtain a high source threshold. Codes with higher source thresholds can be used to compress high-entropy sources without suffering from an error floor caused by the compression. Yet little research has been conducted in jointly designing the components of a code by considering both the source threshold and channel threshold, especially for highentropy sources.

Motivated by the improved source threshold by adding the SVCC linking base matrix and the improved channel threshold by replacing identity matrix in the SCCV linking matrix with a lower or upper triangular base matrix with "1"s on its diagonal, we firstly propose a new type of joint source-channel block codes (JSC-BCs) based on the structure  $\mathbf{B}'_{\mathrm{J}}$  in (3) by adding an SVCC linking matrix to connect the source VNs and channel CNs. Secondly, we simplify the JP-EXIT algorithm to the untransmitted protograph-based EXIT (UP-EXIT) algorithm to calculate the source thresholds of JSC-BCs. Thirdly, we propose a global optimization algorithm based on the UP-EXIT algorithm and the JP-EXIT algorithm to design JSC-BCs by considering both the source and channel thresholds. Theoretical analyses and simulation results both show the proposed codes outperform state-of-the-art DP-LDPC codes for both low-entropy and high-entropy sources. Fourthly, motivated by the superiority of SC-DP-LDPC codes over their corresponding DP-LDPC block codes, we spatially couple the joint source-channel block codes and propose a new type of spatially-coupled joint source-channel codes (SC-JSCC), which can also be constructed based on the SC-DP-LDPC codes by adding a spatially coupled SVCC (SC-SVCC) linking matrix to connect their source variable nodes and channel check nodes. By doing this, SC-JSCCs can achieve higher source thresholds than SC-DP-LDPC codes.

The followings are our main contributions.

- We propose a general structure of a joint source-channel block code (JSC-BC) and present its encoding method. Based on the JP-EXIT algorithm, we provide a simplified algorithm called UP-EXIT algorithm, which only includes source VNs and punctured VNs in the channel protograph in calculating the source threshold of the code.
- 2) We design some new JSC-BCs for sources with different entropies. To save the searching time, we impose some code design rules. We first search for candidate JSC-BCs with high source thresholds by using our proposed UP-EXIT algorithm, and then select the codes among those candidate codes with low channel thresholds by using the JP-EXIT algorithm. By doing this, the search time is saved because of the small protomatrix used in UP-EXIT. Simulation results and theoretical channel thresholds both show the new JSC-BCs outperform existing DP-LDPC block codes.
- 3) We propose a new type of spatially-coupled joint sourcechannel code (SC-JSCC), present its encoding method, and use the sliding window joint BP decoding algorithm to decode the SC-JSCC.
- 4) Based on the JSC-BCs, we construct some new SC-JSCCs. Theoretical analyses and error rate simulation results show that new SC-JSCC codes, whose source, channel, SCCV, and SVCC protomatrices all have spatially coupled structures, can have better error performance than the proposed JSC-BCs and existing SC-DP-LDPC codes. Moreover, the SC-JSCCs can obtain channel thresholds close to the Shannon limit for both low-entropy and highentropy sources.

The structure of this paper is as follows. Section II shows the structure, the encoding method, the protograph-based analysis method, and the design method of the proposed joint source-channel block code (JSC-BC). In the same section, the thresholds and simulation results of the newly constructed JSC-BCs are also presented. In Section III, we introduce the structure and encoding method of the proposed spatially coupled joint source-channel code (SC-JSCC). Based on the JSC-BCs, we construct some SC-JSCCs. Some error performance comparison results are also given in this section. Finally, we give some concluding remarks in Section IV.

## II. PROTOGRAPH-BASED JOINT SOURCE-CHANNEL BLOCK CODE

Fig. 2 illustrates the protograph of the proposed joint sourcechannel block code (JSC-BC). Compared to Fig. 1 which represents the DP-LDPC JSCC system in [23], Fig. 2 involves new connections between VNs in the source protograph and the CNs in the channel protograph. Moreover, it can be denoted by a joint protomatrix, which is denoted by

$$\mathbf{B}_{\mathbf{J}_{\text{new}}} = \begin{pmatrix} \mathbf{B}_{\text{s}} & \mathbf{B}_{\text{sccv}}' \\ \mathbf{B}_{\text{svcc}} & \mathbf{B}_{\text{c}} \end{pmatrix}, \tag{4}$$

where

$$\mathbf{B}_{\mathrm{sccv}}^{'} = \begin{pmatrix} \mathbf{T}_{m_s} & \mathbf{0}_{m_s \times m_c} \end{pmatrix}. \tag{5}$$

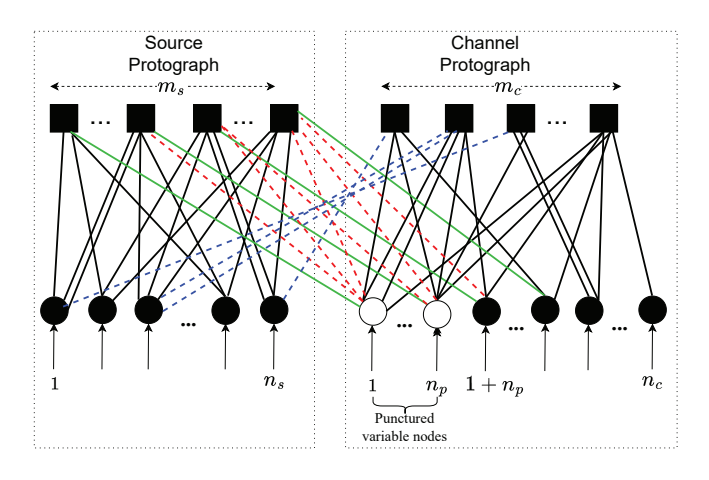


Fig. 2. Protograph representation of joint source-channel block code.

As defined in Section I,  $\mathbf{B}_s$  of size  $m_s \times n_s$  and  $\mathbf{B}_c$  of size  $m_c \times n_c$  are the source protomatrix and the channel protomatrix, respectively.  $\mathbf{T}_{m_s}$  of size  $m_s \times m_s$  is a lower or upper triangular matrix with "1"s on the diagonal.  $\mathbf{B}_{svcc}$  of size  $m_c \times m_s$  is the source-variable-channel-check (SVCC) linking base matrix, which represents the blue connections in Fig. 2.

#### A. Encoder

We lift the protomatrix  $\mathbf{B}_{\mathrm{J}_{\mathrm{new}}}$  to form a large low-density parity-check matrix with a quasi-cyclic structure in two steps. Firstly, we lift  $\mathbf{B}_{\mathrm{J}_{\mathrm{new}}}$  with a relatively small lifting factor  $z_1$  to eliminate all entries with values larger than 1, thereby obtaining a matrix with only 0's and 1's, which is denoted by

$$\mathbf{B}_{\mathbf{J}_{\text{new}}}^{z_1} = \left(\frac{\mathbf{B}_{\mathbf{s}}^{z_1} | \mathbf{T}_{m_s z_1} \mathbf{0}_{m_s z_1 \times m_c z_1}}{\mathbf{B}_{\mathbf{s}}^{z_1} | \mathbf{B}_{\mathbf{c}}^{z_1}}\right). \tag{6}$$

 $\mathbf{B}_{\mathrm{s}}^{z_1}$ ,  $\mathbf{B}_{\mathrm{c}}^{z_1}$ ,  $\mathbf{T}_{m_s z_1}$ , and  $\mathbf{B}_{\mathrm{svcc}}^{z_1}$  are the matrices obtained by lifting  $\mathbf{B}_{\mathrm{s}}$ ,  $\mathbf{B}_{\mathrm{c}}$ ,  $\mathbf{T}_{m_s}$ , and  $\mathbf{B}_{\mathrm{svcc}}$  in the first lifting step, respectively.

Secondly, we lift  $\mathbf{B}_{\mathrm{J}_{\mathrm{new}}}^{z_1}$  with a large lifting factor  $z_2$  to obtain a large parity-check matrix with a quasi-cyclic structure, which is denoted by

$$\mathbf{H}_{\mathbf{J}_{\text{new}}} = \left( \begin{array}{c|c} \mathbf{H}_{\mathbf{s}} & \mathbf{H}_{\mathbf{T}} & \mathbf{0}_{m_s z_1 z_2 \times m_c z_1 z_2} \\ \hline \mathbf{H}_{\text{svcc}} & \mathbf{H}_{\mathbf{c}} \end{array} \right). \tag{7}$$

 $\mathbf{H}_{\mathrm{J}_{\mathrm{new}}}$  contains  $(m_s+m_c)z_1$  rows and  $(n_s+n_c)z_1$  columns of sub-matrices. The submatrix in the i-th row and j-th column is  $\mathbf{I}_{z_2}^{h_{i,j}}$ , which denotes a circulant permutation matrix (CPM) with size  $z_2 \times z_2$  obtained by cyclically right-shifting the identity matrix  $\mathbf{I}_{z_2}$  by  $h_{i,j}$  columns. The second lifting aims to maximize the girth (shortest cycle) of the resultant parity-check matrix.

We use s to denote the source sequence of length  $1 \times N_s = 1 \times n_s z_1 z_2$ . Entries in s are "0" or "1". The probability of "1" in s is denoted by  $p_1$  and the probability of "0" given by  $1-p_1$ . The distribution of "0" and "1" in s follows a Bernoulli distribution. By using the same linear source compression method introduced in [23], we first obtain the compressed source sequence u of length  $1 \times M_s = 1 \times m_s z_1 z_2$  based on  $\left( \begin{array}{c|c} \mathbf{H_s} & \mathbf{H_T} & \mathbf{0}_{m_s z_1 z_2 \times m_c z_1 z_2} \end{array} \right)$ , where  $\mathbf{H_s}$  and  $\mathbf{H_T}$  are,

respectively, the parity-check matrices obtained by lifting  $\mathbf{B}_{\mathrm{s}}^{z_1}$  and  $\mathbf{T}_{m_s z_1}$  in the second lifting step.

Then, we combine s and u as the input for the channel encoder. Next, we generate parity-check bits based on ( $\mathbf{H}_{\mathrm{svcc}} \mid \mathbf{H}_{\mathrm{c}}$ ), where  $\mathbf{H}_{\mathrm{svcc}}$  and  $\mathbf{H}_{\mathrm{c}}$  are the parity-check matrices obtained by lifting  $\mathbf{B}_{\mathrm{svcc}}^{z_1}$  and  $\mathbf{B}_{\mathrm{c}}^{z_1}$ , respectively. The parity-check bits and u (except punctured nodes) are transmitted over the channel. The overall code rate of a JSC-BC is  $R = n_s/(n_c - n_p)$ , where  $n_p$  denotes the number of punctured VNs in  $\mathbf{B}_{\mathrm{c}}$ .

#### B. Calculation of source thresholds

In [16], a source protograph extrinsic information transfer (SPEXIT) algorithm is applied to calculate the source threshold of a double protograph with no connections between VNs in the source P-LDPC code and CNs in the channel P-LDPC code. In [13], a generalized source protograph extrinsic information transfer (GSP-EXIT) algorithm does not consider the case with punctured variable nodes. Thus both algorithms are not suitable for calculating the source thresholds of the proposed JSC-BC. Here, we propose a general algorithm, called the *untransmitted protograph-based EXIT (UP-EXIT) algorithm*, for calculating the source threshold of the proposed JSC-BC. We denote the submatrix corresponding to the untransmitted VNs (i.e., source VNs and punctured channel VNs) by  $\mathbf{B}_{\mathrm{u}}$ , i.e.,

$$\mathbf{B}_{\mathrm{u}} = \begin{pmatrix} \mathbf{B}_{\mathrm{s}} & \mathbf{B}_{\mathrm{sccv}}^{\mathrm{p}} \\ \mathbf{B}_{\mathrm{svcc}} & \mathbf{B}_{\mathrm{p}}^{\mathrm{p}} \end{pmatrix}, \tag{8}$$

where  $\begin{pmatrix} \mathbf{B}_{\mathrm{sccv}}^{\mathrm{p}} \\ \mathbf{B}_{\mathrm{c}}^{\mathrm{p}} \end{pmatrix}$  denotes the first  $n_p$  columns of  $\begin{pmatrix} \mathbf{B}_{\mathrm{sccv}}^{\prime} \\ \mathbf{B}_{\mathrm{c}} \end{pmatrix}$  and corresponds to the  $n_p$  punctured channel VNs. As shown in Fig. 2, we assume that the punctured VNs in the channel protograph are located at the first  $n_p$  VNs of the channel protograph.

We define the following parameters.

- $\mathcal{V} = \{V_1, V_2, ..., V_{n_s+n_c}\}$  denotes the set of VNs in  $\mathbf{B}_{\mathbf{J}_{\mathrm{new}}}$ ;
- $C = \{C_1, C_2, ..., C_{m_s+m_c}\}$  denotes the set of CNs;
- $I_{\text{A-VC}}(i,j)$  denotes the a priori mutual information (AMI) from the j-th VN  $\in \mathcal{V}$  to the i-th CN;
- $I_{\text{A\_CV}}(i,j)$  denotes the AMI from the i-th  $\text{CN} \in \mathcal{C}$  to the j-th  $\text{VN} \in \mathcal{V};$
- $I_{\text{E_CV}}(i,j)$  denotes the extrinsic mutual information (EMI) from the *i*-th CN  $\in \mathcal{C}$  to the *j*-th VN  $\in \mathcal{V}$ ;
- $I_{\mathrm{E\_VC}}(i,j)$  denotes the EMI from the j-th  $\mathrm{VN} \in \mathcal{V}$  to the i-th  $\mathrm{CN}$ ;
- $I_{\text{APP}}(j)$  denotes the MI between the a posteriori probability log-likelihood ratio (APP-LLR) of the j-th  $\text{VN} \in \mathcal{V}$  and its corresponding symbol.

We use  $p_{\rm th}$  to denote the source threshold, i.e., the maximum value of  $p_1$  which allows  $I_{\rm APP}(j)$   $(j=1,2,...,n_s+n_p)$  reaching "1" when the channel information is perfect.

In the traditional joint protograph-based EXIT (JP-EXIT) algorithm [17], the whole protomatrix  $\mathbf{B}_{\mathrm{J}_{\mathrm{new}}}$  is considered. In evaluating the source thresholds of the JSC-BCs, the channel information is assumed to be perfect. In other words, we

can assume that (i)  $I_{\text{A-VC}}(i,j) = I_{\text{E-VC}}(i,j) = 1$  for  $i=1,2,\ldots,m_s+m_c, j=n_s+n_p+1,n_s+n_p+2,\ldots,n_s+n_c;$  and (ii)  $I_{\text{APP}}(j)=1$  for  $j=n_s+n_p+1,\ldots,n_s+n_c.$  Based on the above, the equations in the JP-EXIT algorithm can be simplified. (9) and (10) show the simplified equations used in the UP-EXIT algorithm. Note that only the untransmitted VNs, i.e. source symbols and punctured VNs, and their connected CNs need to be considered in the calculations.

1) EMI transmitted from VNs to CNs is calculated by

$$I_{\text{E\_VC}}(i,j) = \begin{cases} \psi(e_{i,j})J_{\text{BSC}} \left( \sum_{i' \neq i} e_{i',j} [J^{-1}(I_{\text{A\_CV}}(i',j))]^2 + \\ (e_{i,j} - 1)[J^{-1}(I_{\text{A\_CV}}(i,j))]^2, p_1 \right), \\ j = 1, 2, ..., n_s; \forall i, \end{cases}$$

$$\psi(e_{i,j})J \left( \sqrt{\sum_{i' \neq i} e_{i',j} [J^{-1}(I_{\text{A\_CV}}(i',j))]^2} \right),$$

$$+ (e_{i,j} - 1)[J^{-1}(I_{\text{A\_CV}}(i,j))]^2 \right),$$

$$j = n_s + 1, ..., n_s + n_p; \forall i, \end{cases}$$
The state of the (i, i) the estimation  $\mathbf{R}_s$  where  $\mathbf{R}_s$  is the state  $\mathbf{R}_s$  and  $\mathbf{R}_s$  and  $\mathbf{R}_s$  and  $\mathbf{R}_s$  is the state  $\mathbf{R}_s$  and  $\mathbf$ 

where  $e_{i,j}$  denotes the (i,j)-th entry in  $\mathbf{B}_{\mathrm{u}}$ .  $\psi(e_{i,j})=0$  when  $e_{i,j}=0$ , otherwise  $\psi(e_{i,j})=1$ . The definitions of  $J_{\mathrm{BSC}}(\cdot)$ ,  $J(\cdot)$ , and  $J^{-1}(\cdot)$  are given in [13].

2) EMI transmitted from CNs to VNs is updated by

$$I_{\text{E\_CV}}(i,j) = \psi(e_{i,j}) \left( 1 - J \left( \sqrt{\sum_{j' \neq j} e_{i,j'} [J^{-1}(1 - I_{\text{A\_VC}}(i,j'))]^2} \right) + (e_{i,j} - 1)[J^{-1}(1 - I_{\text{A\_VC}}(i,j))]^2 \right) \right),$$

$$j = 1, ..., n_s + n_p; \forall i.$$
(10)

3) MI between the APP-LLRs of VNs and their corresponding symbols is calculated by

$$I_{\text{APP}}(j) = \begin{cases} J_{\text{BSC}}\left(\sum_{i} e_{i,j} [J^{-1}(I_{\text{A\_CV}}(i,j))]^{2}, p_{1}\right), \\ j = 1, 2, ..., n_{s}, \\ J\left(\sqrt{\sum_{i} e_{i,j} [J^{-1}(I_{\text{A\_CV}}(i,j))]^{2}}\right), \\ j = n_{s} + 1, ..., n_{s} + n_{p}. \end{cases}$$
(11)

**Algorithm 1** shows the process of obtaining  $p_{\rm th}$  by using the UP-EXIT algorithm, which is relatively simple compared to the JP-EXIT algorithm. The whole matrix  ${\bf B}_{\rm J_{new}}$  used in JP-EXIT can be reduced to  ${\bf B}_{\rm u}$  for UP-EXIT ( ${\bf B}_{\rm u}$  is the subprotomatrix corresponding to the untransmitted VNs).

#### Algorithm 1 UP-EXIT algorithm based on $B_u$ to find $p_{th}$ .

Given a sub-protomatrix  $\mathbf{B}_{\mathrm{u}}$  shown in (8), set the maximum number of iterations  $l_{max}$ , step size  $\hat{p}_{1}$ , and tolerance value  $\theta$  ( $\theta = 10^{-6}$  in this paper).

Set l = 1 and  $b_{\text{flag}} = \text{flase}$ .

Use a sufficiently large  $p_1 < 0.5$ .

# Start of UP-EXIT algorithm while $b_{\mathrm{flag}} = \mathrm{flase}$ do

```
Set I_{\text{E\_V}_{\text{u}}\text{C}}(i,j) = I_{\text{A\_CV}_{\text{u}}}(i,j) = I_{\text{E\_CV}_{\text{u}}}(i,j) = I_{\text{A\_V}_{\text{u}}\text{C}}(i,j)
= 0 and I_{APP}(j) = 0, i = 1, 2, ..., m_s + m_c, j=1, 2, ...
\ldots, n_s + n_p
Set l=1.
while l \leq l_{max} and b_{flag} = flase do
    Update MI from VNs to CNs by calculating (9).
   Set I_{A V_nC}(i,j) = I_{E V_nC}(i,j) \forall i,j.
   Update MI from CNs to VNs by calculating (10).
    Set I_{A_{\text{CV}_{\text{u}}}}(i,j) = I_{E_{\text{CV}_{\text{u}}}}(i,j) \ \forall i,j.
   Next, calculate I_{APP}(j) by (11).
   if \sum_{j=1}^{n_s+n_p} (1-I_{\mathrm{APP}}(j)) < \theta then Set p_{\mathrm{th}} = p_1 and b_{\mathrm{flag}} = \mathrm{true}.
       End of UP-EXIT algorithm
   else
       Set l = l + 1.
   end if
end while
if b_{\rm flag}= false then
    Set p_1 = p_1 - \hat{p}_1.
end if
```

#### C. Code Design and Results

end while

In this section, we construct some JSC-BCs for low-entropy and high-entropy sources. Source thresholds and channel thresholds can be calculated by using the UP-EXIT algorithm and JP-EXIT algorithm in [17], respectively. The UP-EXIT algorithm requires the use of only the sub-protomatrix corresponding to the untransmitted VNs; whereas the JP-EXIT algorithm requires the use of the complete  $B_{J_{new}}$ . In designing and optimizing  $\mathbf{B}_{\mathrm{J}_{\mathrm{new}}}$ , we apply some existing design rules for DP-LDPC codes [17], [18], [33] and fix the elements of some columns so as to restrict the search space and to reduce the search time. As a result, we only need to design elements in columns corresponding to the untransmitted VNs in  $B_{J_{new}}$ . **Algorithm 2** shows our code design algorithm. Since the subprotomatrices used in UP-EXIT are small, it is easier and faster to find candidate codes with high source thresholds in Step 1). Then, we can find a code with a low channel threshold among these codes in Step 2).

#### Algorithm 2 Optimization of JSC-BCs

- Step 1) Based on the UP-EXIT algorithm, we further use the differential evolution (DE) algorithm [13] to find high-source-threshold sub-protomatrices corresponding to the untransmitted VNs.
- Step 2) Among the candidates found in Step 1), we perform the JP-EXIT algorithm to further find the codes with low channel thresholds. Finally, we select the code with a low channel threshold and a high source threshold.

We compare the following four types of codes. Here,  $\mathbf{B}_{\mathrm{sccv}}^{'} = \begin{pmatrix} \mathbf{T}_{m_s} & \mathbf{0}_{m_s \times m_c} \end{pmatrix}$ ,  $\mathbf{B}_{\mathrm{sccv}} = \begin{pmatrix} \mathbf{I}_{m_s} & \mathbf{0}_{m_s \times m_c} \end{pmatrix}$ , and  $\mathbf{B}_{\mathrm{svcc}}$  is a non-zero protomatrix.

- i) Type-I the proposed JSC-BC in this paper shown in (4), i.e.,  $\mathbf{B}_{\mathrm{J}_{\mathrm{new}}} = \begin{pmatrix} \mathbf{B}_{\mathrm{s}} & \mathbf{B}_{\mathrm{sccv}}' \\ \mathbf{B}_{\mathrm{svcc}} & \mathbf{B}_{\mathrm{c}} \end{pmatrix}$ .
- ii) Type-II the DP-LDPC code  $\mathbf{B}_{\mathrm{J}}^{'} = \begin{pmatrix} \mathbf{B}_{\mathrm{s}} & \mathbf{B}_{\mathrm{sccv}}^{'} \\ \mathbf{0}_{m_{c} \times n_{s}} & \mathbf{B}_{\mathrm{c}}^{'} \end{pmatrix}$  proposed in [23] and shown in (3).  $\mathbf{B}_{\mathrm{J_{a}opt3}}^{0.01}$  and  $\mathbf{B}_{\mathrm{J_{a}opt1}}^{0.04}$  proposed in [23] are codes with structures like  $\mathbf{B}_{\mathrm{J}}^{'}$ .
- iii) Type-III the DP-LDPC code  $\mathbf{B}_{\mathrm{J}}=\begin{pmatrix}\mathbf{B}_{\mathrm{s}}&\mathbf{B}_{\mathrm{sccv}}\\\mathbf{0}_{m_{\mathrm{c}}\times n_{s}}&\mathbf{B}_{\mathrm{c}}\end{pmatrix}$ .  $\mathbf{B}_{\mathrm{J}3}^{0.01}$  [19],  $\mathbf{B}_{\mathrm{J-new}}^{0.01}$  [20], and  $(\mathbf{B}_{\mathrm{s1}},\mathbf{B}_{\mathrm{c1}})$  in [18] are codes with structures like  $\mathbf{B}_{\mathrm{J}}$ .
- iv) Type-IV the DP-LDPC code  $\mathbf{B}_{J}^{*} = \begin{pmatrix} \mathbf{B}_{s} & \mathbf{B}_{sccv} \\ \mathbf{B}_{svcc} & \mathbf{B}_{c} \end{pmatrix}$  proposed in [32].  $\mathbf{B}_{J}^{opti_{-}4}$  [21],  $\mathbf{B}_{J-new_{2}}^{0.04}$  [20],  $(\mathbf{B}_{J3}, \mathbf{B}_{1}^{opt_{-}3})$  [33],  $\mathbf{B}_{1}$  and  $\mathbf{B}_{2}$  in [13],  $\mathbf{B}_{J}^{opti_{-}3}$  [21], and  $\mathbf{B}_{J-new_{2}}^{0.04}$  [20] are codes with structures like  $\mathbf{B}_{J}^{*}$ . Here,  $\mathbf{B}_{1}$  denotes the code consisting of (25) and (26) in [13]; and (25) and (26) in [13] form  $\mathbf{B}_{s}$  and  $\begin{pmatrix} \mathbf{B}_{sccv} \\ \mathbf{B}_{c} \end{pmatrix}$  in  $\mathbf{B}_{J}^{*}$ , respectively; and the first three VNs in the SVCC linking base matrix of  $\mathbf{B}_{1}$  are of degree-2. Similarly,  $\mathbf{B}_{2}$  denotes the code consisting of (19) and (25) in [13]; and (19) and (25) in [13] form  $\mathbf{B}_{s}$  and  $\begin{pmatrix} \mathbf{B}_{sccv} \\ \mathbf{B}_{c} \end{pmatrix}$  of  $\mathbf{B}_{J}^{*}$ , respectively; and the  $\{1,3,5,7\}$ -th VNs in the SVCC linking base matrix of  $\mathbf{B}_{2}$  are of degree-2.
- 1) Low-entropy sources: In this section, we design some codes for low-entropy sources.

Example #1: We consider the DP-LDPC block code designed at  $\overline{p_1}=0.01$  in [23], which is denoted by  $B_{\mathrm{J3~opt3}}^{0.01}$  in (12). Firstly, we add connections between VNs in  $B_{\mathrm{s}}^{0.01}$  and CNs in  $B_{\mathrm{c}}^{0.01}$ . We apply the differential evolution (DE) algorithm [13] based on the JP-EXIT algorithm to optimize these connections, aiming at obtaining a code with a low channel threshold. Additionally, the code obtained should have a higher source threshold than  $B_{\mathrm{J3\_opt3}}^{0.01}$ . Subsequently, we obtain  $B_{\mathrm{Jnew\_0.01}}^{\mathrm{opt1}}$  in (12).

Secondly, we optimize  $\mathbf{B}_{\mathrm{J}_{\mathrm{new}}}$  using **Algorithm 2**. We aim to find a code with a high source threshold and a low channel threshold given  $p_1 = 0.01$ . We fix the elements corresponding to the transmitted channel VNs in  $\mathbf{B}_{\mathrm{J}_{\mathrm{new}}}$ , which include a column with weight-1, two columns with weight-2, and a column with weight-3. Additionally, one VN in  $\mathbf{B}_{\mathrm{s}}$  is assigned with weight-2. Subsequently, we obtain

where x's denote the entries to be determined. As can be seen in (13), x's are located in the four sub-protomatrices (source protomatrix, channel protomatrix, SCCV linking protomatrix,

TABLE I CHANNEL THRESHOLDS AND SOURCE THRESHOLDS OF DIFFERENT CODES AT  $p_1=0.01$ . The Shannon limit equals  $-12.02~\mathrm{dB}$ .

Code	$\mathbf{B}_{\mathrm{J}_{\mathrm{new\_0.01}}}^{\mathrm{opt1}}$	$\mathbf{B}_{\mathrm{J}_{\mathrm{new\_0.01}}}^{\mathrm{opt2}}$	${f B}_{{ m J3\_opt3}}^{0.01}$ [23]	<b>B</b> <sub>J3</sub> <sup>0.01</sup> [19, Table I]	<b>B</b> <sup>0.01</sup> <sub>J-new</sub> [20, Table II]
$(E_s/N_0)_{\rm th}$ (dB)	-9.787	-10.170	-9.734	-9.324	-9.725
$p_{ m th}$	0.041	0.084	0.028	0.028	0.028

TABLE II Channel thresholds and source thresholds of different codes at  $p_1=0.04$ . The Shannon limit equals  $-7.00~{\rm dB}$ .

Code	$\mathbf{B}_{\mathrm{J}_{\mathrm{new\_0.04}}}^{\mathrm{opt1}}$	$\mathbf{B}_{\mathrm{J}_{\mathrm{new\_0.04}}}^{\mathrm{opt2}}$	${f B}_{ m J_opt1}^{0.04}$ [23]	$(\mathbf{B}_{\mathrm{s1}}, \mathbf{B}_{\mathrm{c1}})$ in [18, Table I]	<b>B</b> <sub>J</sub> <sup>opti_4</sup> [21]	$(\mathbf{B}_{\mathrm{J-new2}}^{0.04})$ [20, Table I]
$(E_s/N_0)_{\rm th}$ (dB)	-5.202	-5.880	-5.267	-5.135	-5.568	-5.729
$p_{ m th}$	0.137	0.217	0.082	0.063	0.137	0.129

and SVCC linking protomatrix) of  $\mathbf{B}_{\mathrm{J_{new}}}$ . The maximum value of x is set as 3. The first VN in the channel code is the punctured VN and its degree should be the largest. As shown in [23], the decoding complexity is related to the maximum row weight. (Unless otherwise stated, we use the joint BP algorithm [21] to decode the JSC-BC codes.) Based on our observations of existing DP-LDPC codes designed at  $p_1=0.01$ , we set the maximum row weight to 16 as to maintain the same decoding complexity as (12). By using **Algorithm 2** to search for x's in (13), we obtain

Table I compares the source and channel thresholds of JSC-BCs designed at  $p_1=0.01$  and state-of-the-art DP-LDPC block codes designed at  $p_1=0.01$  [19], [20], [23]. We can see that  ${\bf B}_{{\rm J}_{\rm new\_0.01}}^{\rm opt2}$  has a lower channel threshold and a higher source threshold than  ${\bf B}_{{\rm J}_{\rm new\_0.01}}^{\rm opt1}$ .  ${\bf B}_{{\rm J}_{\rm new\_0.01}}^{\rm opt2}$  also achieves lower channel thresholds and higher source thresholds than state-of-the-art DP-LDPC block codes. Fig. 3 plots the source symbol error rate (SSER) performance of these codes under different  $E_s/N_0$  (in dB).  $E_s/N_0$  denotes the average-energy-transmitted-per-source-symbol-to-noise-power-spectral-density. We can see that  ${\bf B}_{{\rm J}_{\rm new\_0.01}}^{\rm opt2}$  has a gain of about 0.12 dB over  ${\bf B}_{{\rm J}_{\rm new\_0.01}}^{\rm opt1}$  at an SSER of  $10^{-6}$ . It has gains of about 0.25 dB over  ${\bf B}_{{\rm J}_{\rm Jopt3}}^{\rm opt3}$  [23] at an SSER of  $10^{-6}$ . B $_{{\rm J}_{\rm new\_0.01}}^{\rm opt1}$  also has better error performance than  ${\bf B}_{{\rm J}_{\rm Jopt3}}^{0.01}$ . The SSER results are consistent with the theoretical channel thresholds given in Table I.

Example #2: We consider the code designed at  $p_1 = 0.04$  in  $\overline{[23]}$ , which is denoted by  $\mathbf{B}_{\mathrm{J_{opt}1}}^{0.04}$  in (15). Similar to Example #1, we firstly add and optimize connections between VNs in  $\mathbf{B}_{\mathrm{s}}^{0.04}$  and CNs in  $\mathbf{B}_{\mathrm{c}}^{0.04}$ , and obtain  $\mathbf{B}_{\mathrm{J_{new_{-0.04}}}}^{\mathrm{opt1}}$  in (15).

$$\begin{split} \mathbf{B}_{\mathrm{J\_opt1}}^{0.04} &= & \mathbf{B}_{\mathrm{J_{new\_0.04}}}^{\mathrm{opt1}} = \\ \begin{pmatrix} 1 & 1 & 1 & 2 & | & 1 & 0 & 0 & 0 & 0 \\ 1 & 2 & 2 & 1 & | & 1 & 1 & 0 & 0 & 0 \\ \hline 0 & 0 & 0 & 0 & | & 2 & 2 & 1 & 0 & 1 \\ 0 & 0 & 0 & 0 & | & 1 & 1 & 0 & 1 & 1 \\ 0 & 0 & 0 & 0 & | & 2 & 0 & 0 & 1 & 1 \end{pmatrix} \text{ and } \begin{pmatrix} 1 & 1 & 1 & 2 & | & 1 & 0 & 0 & 0 & 0 \\ \hline 1 & 2 & 2 & 1 & | & 1 & 1 & 0 & 0 & 0 & 0 \\ \hline 0 & 0 & 0 & 1 & | & 2 & 2 & 1 & 0 & 1 & 1 \\ 0 & 0 & 0 & 0 & | & 1 & 1 & 0 & 1 & 1 \\ 0 & 0 & 0 & 0 & | & 2 & 0 & 0 & 1 & 1 \end{pmatrix}. \end{split}$$
 (15)

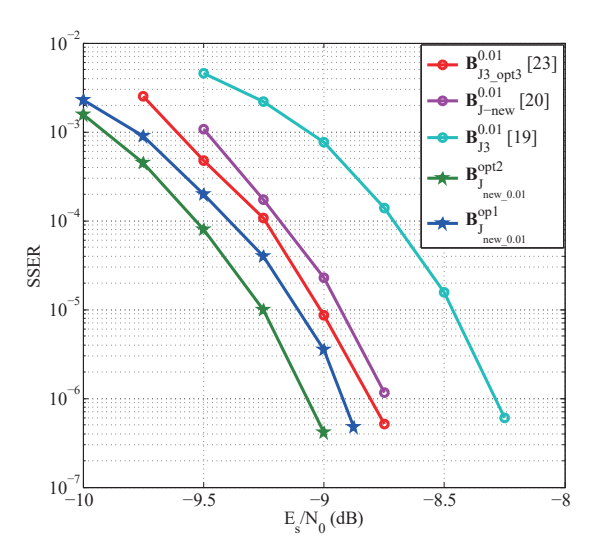


Fig. 3. SSER performance comparison between  ${\bf B}_{\rm Jnew,0.01}^{\rm opt1}, {\bf B}_{\rm Jnew,0.01}^{\rm opt2},$  and state-of-the-art DP-LDPC block codes at  $p_1=0.01$ . The lifting factor is  $z=z_1z_2=4\times400=1600$ .

Secondly, we optimize  $\mathbf{B}_{\mathrm{J}_{\mathrm{new}}}$  using **Algorithm 2**. We aim to find a code with a high source threshold and a low channel threshold given  $p_1 = 0.04$ . Similar to Example #1, we fix the elements corresponding to the transmitted channel VNs and the elements corresponding to one source VN, and we obtain

$$\mathbf{B}_{\text{Jnew}}^{0.04} = \begin{pmatrix} 1 & x & x & 1 & 0 & 0 & 0 & 0 \\ 1 & x & x & x & 1 & 0 & 0 & 0 \\ \hline 0 & x & x & x & x & 0 & 1 & 0 & 0 \\ 0 & x & x & x & x & 0 & 1 & 0 & 0 \\ 0 & x & x & x & x & 1 & 0 & 0 & 1 & 2 \end{pmatrix}. \tag{16}$$

Based on our observations of existing DP-LDPC codes designed at  $p_1 = 0.04$ , we set the maximum row weight to 8 as to maintain the same decoding complexity as (15). By using **Algorithm 2** to search for x's in (16), we obtain

$$\mathbf{B}_{\mathbf{J}_{\text{new\_0.04}}}^{\text{opt2}} = \begin{pmatrix} 1 & 0 & 2 & 3 & 1 & 0 & 0 & 0 & 0 \\ 1 & 1 & 1 & 1 & 3 & 1 & 0 & 0 & 0 \\ \hline 0 & 0 & 0 & 1 & 3 & 0 & 1 & 0 & 0 \\ 0 & 0 & 0 & 0 & 3 & 0 & 0 & 1 & 1 \\ 0 & 2 & 0 & 0 & 1 & 1 & 0 & 1 & 2 \end{pmatrix}. \tag{17}$$

Table II compares the source and channel thresholds of the constructed JSC-BCs and state-of-the-art DP-LDPC block codes designed at  $p_1 = 0.04$  [18], [20], [21], [23]. We can see

TABLE III Channel thresholds and source thresholds of different codes at  $p_1=0.10$  and  $p_1=0.20$ .

$p_1$		0.10							0.20		
Code	$\mathbf{B}^{\mathrm{opt1}}_{\mathrm{J}_{\mathrm{new\_0.10}}}$	$\mathbf{B}^{\mathrm{opt2}}_{\mathrm{J}_{\mathrm{new\_0.10}}}$	$(\mathbf{B}_{J3}, \mathbf{B}_{l}^{opt-3})$ [33]	$\mathbf{B}_{1}$ [13]	$\mathbf{B}_{\mathrm{J}}^{\mathrm{opti}\_3}$ [21]	( <b>B</b> <sup>0.04</sup> <sub>J-new2</sub> ) [20, Table I]	$\mathbf{B}^{\mathrm{opt1}}_{\mathrm{J}_{\mathrm{new\_0.20}}}$	$\mathbf{B}^{\mathrm{opt2}}_{\mathrm{J}_{\mathrm{new\_0.20}}}$	$\mathbf{B}_{2}$ [13]		
$(E_s/N_0)_{\rm th}$ (dB)	-2.333	-2.595	-1.556	-1.581	-1.996	-1.218	1.048	0.831	2.322		
$p_{ m th}$	0.137	0.171	0.159	0.160	0.144	0.129	0.334	0.288	0.283		
The Shannon limit (dB)		-3.392						-0.654			

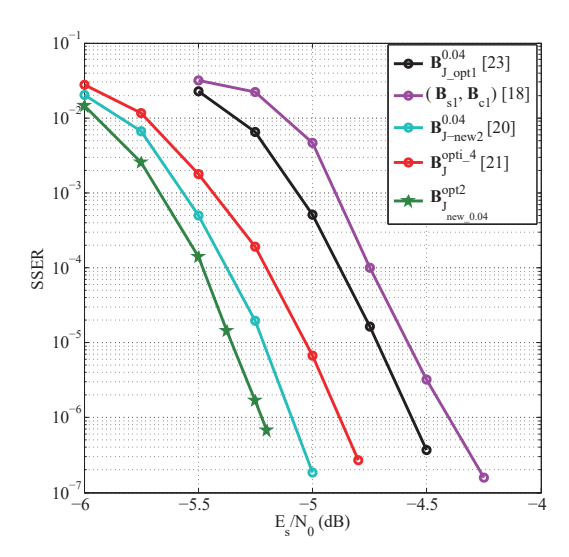


Fig. 4. SSER performance comparison between  ${\bf B}_{{\rm J}_{\rm new},0.04}^{\rm opt1}, {\bf B}_{{\rm J}_{\rm new},0.04}^{\rm opt2}$ , and state-of-the-art DP-LDPC block codes at  $p_1=0.04$ . The lifting factor is  $z=z_1z_2=4\times 800=3200$ .

that  $B_{J_{\rm new\_0.04}}^{\rm opt2}$  achieves lower channel thresholds and higher source threshold than  $B_{J_{\rm new\_0.04}}^{\rm opt1}$  and state-of-the-art DP-LDPC block codes. Fig. 4 plots the SSER performance of these codes. We can see that  $B_{J_{\rm new\_0.04}}^{\rm opt2}$  has the best error performance among all codes.  $B_{J_{\rm new\_0.04}}^{\rm opt2}$  has a gain of about 0.75 dB over  $B_{J_{\rm new\_0.04}}^{\rm opt1}$  at an SSER of  $10^{-6}$ . It has gains of about 0.1 dB and 0.3 dB, respectively, over  $B_{J_{\rm new_0.04}}^{0.04}$  [20] and  $B_{J}^{\rm opt1}$  [21] at an SSER of  $10^{-6}$ . Note that  $B_{J_{\rm new\_0.04}}^{\rm opt1}$  has a worse error performance than  $B_{J_{\rm opt1}}^{0.04}$  [23], which is consistent with its theoretical channel threshold being higher than that of  $B_{J_{\rm opt1}}^{0.04}$ . The results indicate that by directly adding a non-zero SVCC linking base matrix to an existing DP-LDPC code, the channel threshold and error performance of the resultant code may become worse even though its source threshold becomes higher.

2) High-entropy sources: In this section, we design some codes for high-entropy sources.

Example #3: According to Shannon's coding theory,  $R\overline{H(p_1)} < 1$ , where  $H(p_1) = -p_1 \log_2 p_1 - (1-p_1) \log_2 (1-p_1)$  is the source entropy. When  $H(p_1)$  is relatively large, R needs to be relatively small. In this paper, we set  $p_1 = 0.10, 0.20$  and R = 1. Firstly, we optimize the SVCC linking

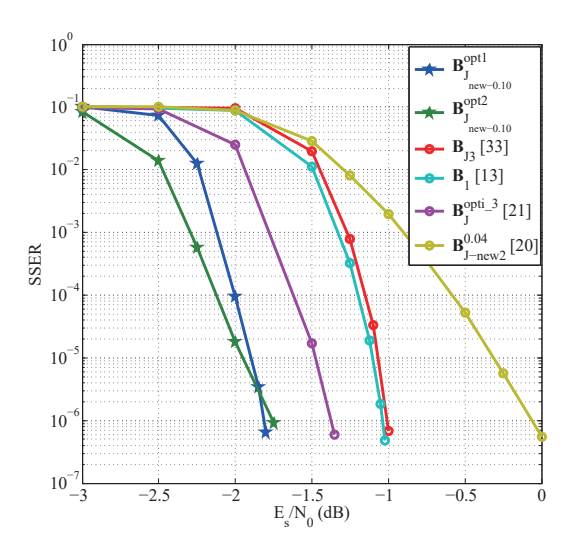


Fig. 5. SSER performance comparison between  ${\bf B}_{\rm Jnew,0.10}^{\rm opt1}, {\bf B}_{\rm Jnew,0.10}^{\rm opt2},$  and existing DP-LDPC block codes at  $p_1=0.10$ . The lifting factor is  $z=z_1z_2=4\times 800=3200$ .

base matrix based on (15) and obtain

$$\begin{array}{lll} \mathbf{B}_{J_{\mathrm{new}\_0.10}}^{\mathrm{opt1}} = & \mathbf{B}_{J_{\mathrm{new}\_0.20}}^{\mathrm{opt1}} = \\ \begin{pmatrix} 1 \ 1 \ 1 \ 2 \ | \ 1 \ 0 \ 0 \ 0 \ 0 \\ \hline 0 \ 0 \ 0 \ 0 \ | \ 2 \ 2 \ 1 \ 0 \ 1 \\ 0 \ 0 \ 0 \ | \ 1 \ 1 \ 1 \ 0 \ 1 \\ 0 \ 0 \ 0 \ | \ 2 \ 0 \ 0 \ 1 \ 1 \end{pmatrix} & \text{and} & \begin{pmatrix} 1 \ 1 \ 1 \ 2 \ | \ 1 \ 0 \ 0 \ 0 \ 0 \\ \hline 0 \ 1 \ 1 \ 0 \ 2 \ 2 \ 1 \ 0 \ 1 \\ \hline 0 \ 1 \ 0 \ 0 \ 1 \ 1 \ 0 \ 1 \ 0 \\ \hline 0 \ 1 \ 0 \ 0 \ 1 \ 1 \ 0 \ 1 \ 1 \\ \hline 0 \ 0 \ 0 \ 0 \ 2 \ 0 \ 0 \ 1 \ 1 \end{pmatrix}. \end{array} \tag{18}$$

for  $p_1 = 0.10$  and  $p_1 = 0.20$ , respectively.

Next, by using **Algorithm 2**, we search for x's in (16) given  $p_1 = 0.10$  and 0.20, respectively, and obtain

$$\begin{array}{lll} \mathbf{B}_{\mathrm{J}_{\mathrm{new}\_0.10}}^{\mathrm{opt2}} = & & \mathbf{B}_{\mathrm{J}_{\mathrm{new}\_0.20}}^{\mathrm{opt2}} = \\ \begin{pmatrix} 1 \ 0 \ 3 \ 0 \ | \ 1 \ 0 \ 0 \ 0 \ 0 \\ \hline 0 \ 0 \ 0 \ 0 \ | \ 3 \ 0 \ 1 \ 0 \ 0 \\ \hline 0 \ 2 \ 0 \ | \ | \ 2 \ 0 \ 0 \ 1 \\ \hline 0 \ 0 \ 2 \ 1 \ | \ 1 \ 0 \ 0 \ 1 \\ \hline 0 \ 0 \ 2 \ 1 \ | \ 1 \ 0 \ 0 \ 1 \\ \hline 0 \ 0 \ 0 \ 1 \ | \ 1 \ 0 \ 0 \ 1 \\ \hline 0 \ 0 \ 0 \ 1 \ | \ 1 \ 0 \ 0 \ 1 \\ \hline \end{array} \right). \end{array} \quad \text{(19)}$$

Table III lists the source and channel thresholds of  $\mathbf{B}_{J_{\mathrm{new\_0.10}}}^{\mathrm{opt1}}$ ,  $\mathbf{B}_{J_{\mathrm{new\_0.10}}}^{\mathrm{opt2}}$ , and existing DP-LDPC block codes with non-zero SVCC linking base matrices [13], [20], [21], [33] at  $p_1=0.10$ . It can be seen that given  $p_1=0.10$ ,  $\mathbf{B}_{J_{\mathrm{new\_0.10}}}^{\mathrm{opt2}}$  have lower channel thresholds than  $\mathbf{B}_{J_{\mathrm{new\_0.10}}}^{\mathrm{opt1}}$  and existing DP-LDPC codes. Fig. 5 plots the SSER performance of these codes. The two new codes  $\mathbf{B}_{J_{\mathrm{new\_0.10}}}^{\mathrm{opt1}}$  and  $\mathbf{B}_{J_{\mathrm{new\_0.10}}}^{\mathrm{opt2}}$  have a maximum gain of around 1.7 dB and a minimum gain of about 0.5 dB over the existing codes at an SSER of  $10^{-6}$ .  $\mathbf{B}_{J_{\mathrm{new\_0.10}}}^{\mathrm{opt2}}$  has better error performance than  $\mathbf{B}_{J_{\mathrm{new\_0.10}}}^{\mathrm{opt1}}$ . The SSER results are also consistent with the theoretical thresholds in Table III.

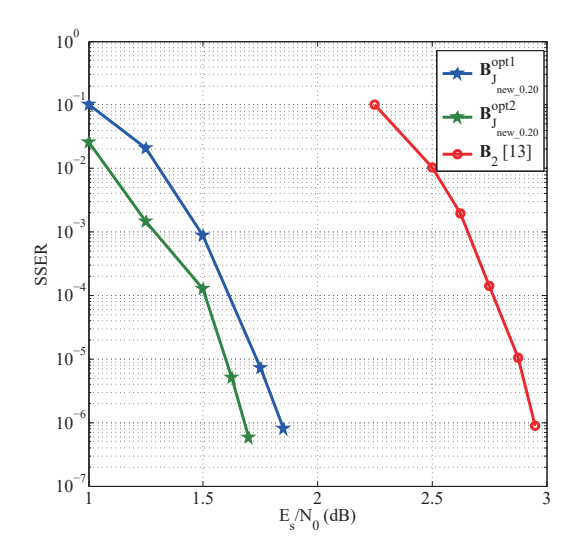


Fig. 6. SSER performance comparison between  $\mathbf{B}_{\mathrm{J_{new}},0.20}^{\mathrm{opt1}}$ ,  $\mathbf{B}_{\mathrm{J_{new}},0.20}^{\mathrm{opt2}}$ , and an existing DP-LDPC block code  $\mathbf{B}_2$  at  $p_1=0.20$ . The lifting factor is  $z=z_1z_2=4\times800=3200$ .

Table III also lists the source and channel thresholds of  ${\bf B}_{{\rm J}_{{\rm new}_0.20}}^{\rm pt1}$ ,  ${\bf B}_{{\rm J}_{{\rm new}_0.20}}^{\rm pt2}$ , and  ${\bf B}_2$  (a DP-LDPC block code with a non-zero SVCC linking base matrix in [13]) at  $p_1=0.20$ . It can be seen that given  $p_1=0.20$ ,  ${\bf B}_{{\rm J}_{{\rm new}_0.20}}^{\rm opt1}$  and  ${\bf B}_{{\rm J}_{{\rm new}_0.20}}^{\rm opt2}$  achieve lower channel thresholds than  ${\bf B}_2$ .  ${\bf B}_{{\rm J}_{{\rm new}_0.20}}^{\rm opt2}$  has a channel threshold 0.217 dB lower than  ${\bf B}_{{\rm J}_{{\rm new}_0.20}}^{\rm opt1}$ . Fig. 6 plots the SSER performance of these codes. The new codes  ${\bf B}_{{\rm J}_{{\rm new}_0.20}}^{\rm opt1}$  and  ${\bf B}_{{\rm J}_{{\rm new}_0.20}}^{\rm opt2}$  significantly outperform the existing one  ${\bf B}_2$ . Moreover,  ${\bf B}_{{\rm J}_{{\rm new}_0.20}}^{\rm opt2}$  has a gain of more than 0.15 dB over  ${\bf B}_{{\rm J}_{{\rm new}_0.20}}^{\rm opt1}$  at an SSER of  $10^{-6}$ .

Based on the examples above, we can observe that our proposed codes outperform the other three types of codes. It is because the design of our proposed code structure is more flexible and is therefore more likely to find a code having good thresholds and good error performance.

## III. PROTOGRAPH-BASED SPATIALLY-COUPLED JOINT SOURCE-CHANNEL CODE

In [29], a source spatially coupled protograph-based LDPC (SC-P-LDPC) code and a channel SC-P-LDPC code are concatenated. In [30], a source SC-P-LDPC code and a channel SC-P-LDPC code are spatially coupled by using a spatiallycoupled SCCV (SC-SCCV) linking (base) matrix; in other words, the source SC-P-LDPC code and the channel SC-P-LDPC code are not connected in a simple cascading relationship. In this paper, we propose a new type of spatially coupled joint source-channel code (SC-JSCC). In the proposed SC-JSCC, a source SC-P-LDPC code and a channel SC-P-LDPC code are not only spatially coupled by a SC-SCCV linking (base) matrix, but also by a spatially-coupled SVCC (SC-SVCC) linking (base) matrix. By doing this, we aim to improve the source threshold without changing the source compression rate or increasing the syndrome former memory of the source SC-P-LDPC proposed in [29].

Fig. 7 shows the protomatrix of the proposed SC-JSCC  ${f B}_{\rm TD}$  and the corresponding parity-check matrix  ${f H}_{\rm TD}$  formed

by lifting  $\mathbf{B}_{\mathrm{TD}}$  twice.  $m_0,\ m_1,\ m_2,\$ and  $m_3,\$ respectively, represent the syndrome former memories of the source SC-P-LDPC code, the channel SC-P-LDPC code, the SC-SCCV linking matrix, and the SC-SVCC linking matrix.  $L_s$  and  $L_c$ , respectively, denote the coupling lengths of the source and channel SC-P-LDPC codes. When  $L_s$  and  $L_c$  are finite, the corresponding code is called spatially-coupled joint source-channel (SC-JSC) terminated code. When both  $L_s$  and  $L_c$  tend to infinity, the SC-JSCC becomes a spatially-coupled joint source-channel convolutional code (SC-JSC-CC). For the SC-JSC-CC, its overall code rate  $R_{\mathrm{CC}}=R$ . For the SC-JSC terminated code,  $R_{\mathrm{TD}}=L_s/L_c\cdot R_{\mathrm{CC}}< R_{\mathrm{CC}}$ .

The sub-base matrices  $\mathbf{B}_{s_i}$   $(i=0,1,\ldots,m_0)$ ,  $\mathbf{B}_{c_i}$   $(i=0,1,\ldots,m_1)$ , and  $\mathbf{B}_{svcc_i}$   $(i=0,1,\ldots,m_3)$  can, respectively, be constructed from  $\mathbf{B}_s$ ,  $\mathbf{B}_c$ , and  $\mathbf{B}_{svcc}$  in  $\mathbf{B}_{J_{new}}$  (4). Moreover, they need to satisfy  $\sum_{i=0}^{m_0} \mathbf{B}_{s_i} = \mathbf{B}_s$ ,  $\sum_{i=0}^{m_1} \mathbf{B}_{c_i} = \mathbf{B}_c$ , and  $\sum_{i=0}^{m_3} \mathbf{B}_{svcc_i} = \mathbf{B}_{svcc}$  [34]. We further require  $\mathbf{B}_{c_0} = (\mathbf{B}_{m_c \times m_s} \ \mathbf{T}_{m_c})$ , where  $\mathbf{B}_{m_c \times m_s}$  is a base matrix of size  $m_c \times m_s$  and  $\mathbf{T}_{m_c}$  of size  $m_c \times m_c$  denotes a lower or upper triangular protomatrix with "1"s on its diagonal such that linear encoding can be implemented. For the SC-SCCV linking matrix, we require  $\mathbf{B}_{sccv_0}$  to have the same structure as  $\mathbf{B}'_{sccv}$  (i.e.,  $= (\mathbf{T}_{m_s} \ \mathbf{0})$ ) in  $\mathbf{B}_{J_{new}}$  (4) so as to allow linear source compression. We can divide the proposed SC-JSCC into two categories based on the sub-matrices of the SC-SCCV linking matrix:

- 1) Type-I all  $\mathbf{B}_{\mathrm{sccv}_i}$   $(i=1,2,...,m_2)$  are zero matrices;
- 2) Type-II not all  $\mathbf{B}_{\mathrm{sccv}_i}$  ( $i=1,2,...,m_2$ ) are zero matrices.

Remark: For Type-II SC-JSCCs, the corresponding DP-LDPC block codes may not exist. Given a set of  $\mathbf{B}_{\mathrm{sccv}_i}$  ( $i=0,1,2,...,m_2$ ), where  $\mathbf{B}_{\mathrm{sccv}_0}=\begin{pmatrix}\mathbf{T}_{m_s}&\mathbf{0}\end{pmatrix}$  and not all  $\mathbf{B}_{\mathrm{sccv}_i}$  ( $i=1,2,...,m_2$ ) are zero matrices,  $\sum_{i=0}^{m_2}\mathbf{B}_{\mathrm{sccv}_i}$  may not obey the structure of  $\mathbf{B}_{\mathrm{sccv}}'$  in  $\mathbf{B}_{\mathrm{Jnew}}$  (4), i.e., consisting of a lower or upper triangular protomatrix of size  $m_s\times m_s$  with "1"s on the diagonal and a zero matrix. Therefore, we do not base on  $\mathbf{B}_{\mathrm{sccv}}'$  to construct the SC-SCCV linking base matrix for Type-II SC-JSCCs.

#### A. Encoder

At time  $t \ (= 0, 1, 2, \ldots)$ , the source sequence of size  $1 \times n_s z$  (z is the overall lifting factor) is denoted by  $s_t$ . The compressed source sequence of size  $1 \times m_s z$  is denoted by  $c_t$  at time t. The parity-check bit sequence of size  $1 \times m_c z$  for channel encoder is denoted by  $p_t$  at time t. The channel codeword sequence of size  $1 \times n_c z$  is denoted by  $v_t$  at time t. We assume  $m_0 = m_1 = m_2 = m_3$  to simplify the explanation.

At t = 0, we generate the codeword  $v_0$  based on the input  $s_0$  and the parity-check matrix

$$\begin{pmatrix}
s_0 & v_0 = [c_0 & p_0] \\
\frac{\mathbf{H}_{s_0} & \mathbf{H}_{sccv_0}}{\mathbf{H}_{svcc_0} & \mathbf{H}_{c_0}}
\end{pmatrix} , (20)$$

where  $\mathbf{H}_{s_0}$ ,  $\mathbf{H}_{c_0}$ ,  $\mathbf{H}_{sccv_0}$ , and  $\mathbf{H}_{svcc_0}$  are, respectively, on the 1st block rows of  $\mathbf{H}_{TD}^s$ ,  $\mathbf{H}_{TD}^c$ ,  $\mathbf{H}_{TD}^{sccv}$ , and  $\mathbf{H}_{TD}^{svcc}$  in Fig. 7.  $\mathbf{H}_{sccv_0}$  is formed by lifting  $\mathbf{B}_{sccv_0} = (\mathbf{T}_{m_s} \quad \mathbf{0})$  twice. We

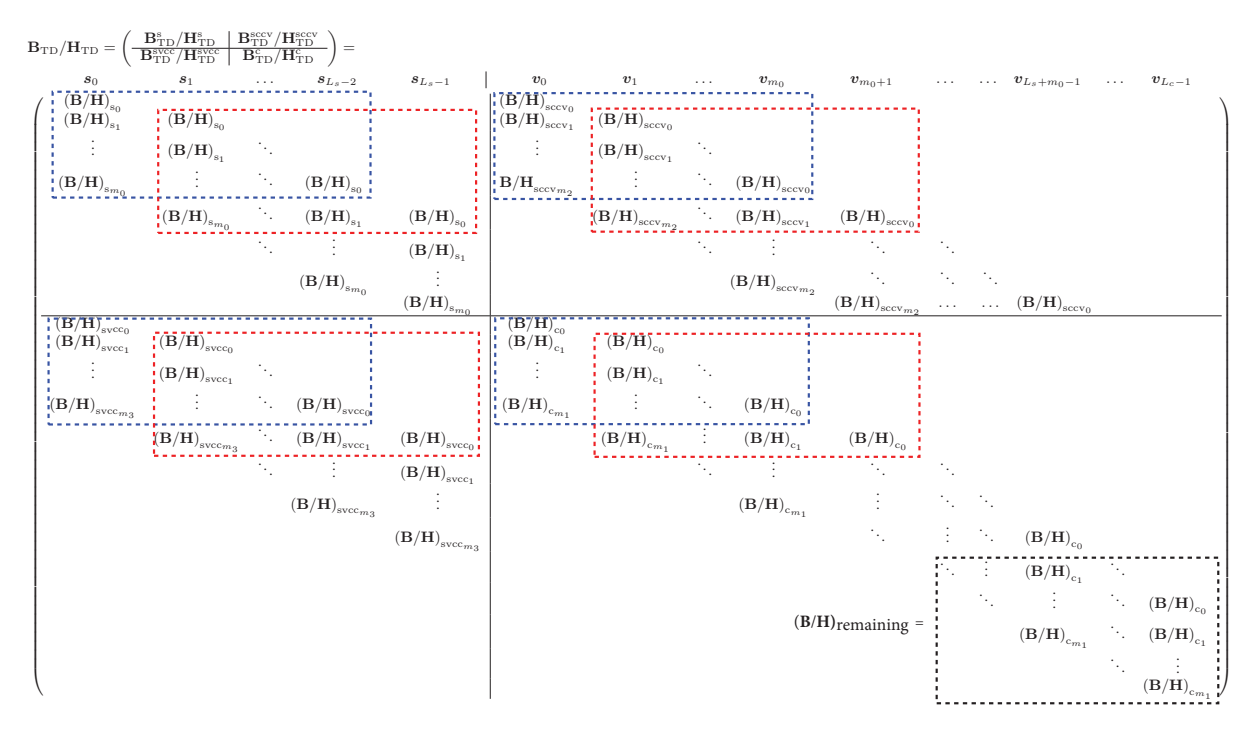


Fig. 7. Protomatrix and parity-check matrix of proposed spatially coupled joint source-channel codes are denoted by  $\mathbf{B}_{\mathrm{TD}}$  and  $\mathbf{H}_{\mathrm{TD}}$ , respectively. When  $L_s$  and  $L_c$  are infinite, the corresponding code is called spatially coupled joint source-channel convolutional code

can obtain  $v_0$  by using the similar encoding method as described for the JSC-BC in Section II-A. Firstly,  $c_0$  is computed based on  $s_0$  and  $(\mathbf{H}_{s_0} \mid \mathbf{H}_{sccv_0})$  by using the linear source compression [23]. Then,  $p_0$  is computed based on (i)  $c_0$  and  $s_0$ ; and (ii)  $(\mathbf{H}_{svcc_0} \mid \mathbf{H}_{c_0})$  by using linear encoding method. (Recall that  $\mathbf{H}_{c_0}$  is formed by lifting  $\mathbf{B}_{c_0} = (\mathbf{B}_{m_c \times m_s} \quad \mathbf{T}_{m_c})$  twice.)

At  $0 < t < m_0$ , the source sequence  $s_t$  is input into the encoder.  $v_t$  is generated by using the similar encoding method as described in Section II-A based on the known  $s_0, \ldots, s_t$  and  $v_0, \ldots, v_{t-1}$  and the following parity-check matrix

$$\begin{pmatrix} \mathbf{s}_0 & \cdots & \mathbf{s}_{t-1} & \mathbf{s}_t & \mathbf{v}_0 & \cdots & \mathbf{v}_{t-1} & \mathbf{v}_t = [\mathbf{c}_t & \mathbf{p}_t] \\ \frac{\mathbf{H}_{\mathbf{s}_t} & \cdots & \mathbf{H}_{\mathbf{s}_1} & \mathbf{H}_{\mathbf{s}_0} & \mathbf{H}_{\mathbf{sccv}_t} \cdots \mathbf{H}_{\mathbf{sccv}_1} & \mathbf{H}_{\mathbf{sccv}_0} \\ \overline{\mathbf{H}_{\mathbf{svcc}_t} \cdots \mathbf{H}_{\mathbf{svcc}_1} \mathbf{H}_{\mathbf{svcc}_0} & \mathbf{H}_{\mathbf{c}_t} & \cdots & \mathbf{H}_{\mathbf{c}_1} & \mathbf{H}_{\mathbf{c}_0} \end{pmatrix} , \quad (21)$$

where  $\mathbf{H}_{\mathrm{s}_i}$ ,  $\mathbf{H}_{\mathrm{c}_i}$ ,  $\mathbf{H}_{\mathrm{sccv}_i}$ , and  $\mathbf{H}_{\mathrm{svcc}_i}$  ( $i=0,1,\ldots,t$ ) are, respectively, on the (t+1)-th block rows of  $\mathbf{H}_{\mathrm{TD}}^{\mathrm{s}}$ ,  $\mathbf{H}_{\mathrm{TD}}^{\mathrm{c}}$ ,  $\mathbf{H}_{\mathrm{TD}}^{\mathrm{sccv}}$ , and  $\mathbf{H}_{\mathrm{TD}}^{\mathrm{svcc}}$  in Fig. 7.

At  $t \geq m_0$  ( $m_0 \leq t \leq L_s - 1$  for SC-JSCCs), the source sequence  $s_t$  is input into the encoder.  $v_t$  is generated based on the known  $s_{t-m_0}, \ldots, s_t$  and  $v_{t-m_0}, \ldots, v_{t-1}$  and the following parity-check matrix

$$\begin{pmatrix} \mathbf{s}_{t-m_0} & \cdots & \mathbf{s}_{t-1} & \mathbf{s}_t & \mathbf{v}_{t-m_0} & \cdots & \mathbf{v}_{t-1} & \mathbf{v}_t = [\mathbf{c}_t & \mathbf{p}_t] \\ \mathbf{H}_{\mathrm{S}m_0} & \cdots & \mathbf{H}_{\mathrm{s}_1} & \mathbf{H}_{\mathrm{s}_0} & \mathbf{H}_{\mathrm{SCCv}_{m_2}} & \cdots & \mathbf{H}_{\mathrm{SCCv}_1} \\ \mathbf{H}_{\mathrm{svcc}_{m_3}} & \cdots & \mathbf{H}_{\mathrm{svcc}_1} & \mathbf{H}_{\mathrm{svcc}_0} | & \mathbf{H}_{\mathbf{c}_{m_1}} & \cdots & \mathbf{H}_{\mathbf{c}_1} & \mathbf{H}_{\mathbf{c}_0} \end{pmatrix} ,$$

$$(22)$$

where  $\mathbf{H}_{\mathrm{s}i}$ ,  $\mathbf{H}_{\mathrm{c}i}$ ,  $\mathbf{H}_{\mathrm{sccv}i}$ , and  $\mathbf{H}_{\mathrm{svcc}i}$  ( $i=0,1,\ldots,m_0$  and  $m_0=m_1=m_2=m_3$ ) are, respectively, on the (t+1)-th block rows of  $\mathbf{H}_{\mathrm{TD}}^{\mathrm{s}}$ ,  $\mathbf{H}_{\mathrm{TD}}^{\mathrm{c}}$ ,  $\mathbf{H}_{\mathrm{TD}}^{\mathrm{sccv}}$ , and  $\mathbf{H}_{\mathrm{TD}}^{\mathrm{svcc}}$  in Fig. 7.

When SC-JSCCs are terminated,  $v_{L_s}, ..., v_{L_c}$  are generated without any new inputs.

1) Firstly, we continue to generate the channel codewords  $v_{L_s}, ..., v_{L_s+m_0-1}$ . Specifically, we generate  $v_{L_s-1+j}$ 

 $(j=1,...,m_0)$  based on the known  $s_{L_s-m_0-1+j},...,s_{L_s-1},v_{L_s-m_2-1+j},...,v_{L_s-2+j}$  and the following parity-check matrix

where  $(\mathbf{H}_{\mathbf{s}_{m_0}}, ..., \mathbf{H}_{\mathbf{s}_j})$ ,  $(\mathbf{H}_{\mathbf{svcc}_{m_3}}, ..., \mathbf{H}_{\mathbf{svcc}_j})$ ,  $\mathbf{H}_{\mathbf{c}_i}$ , and  $\mathbf{H}_{\mathbf{sccv}_i}$   $(i=0,...,m_0; m_0=m_1=m_2=m_3)$  are, respectively, on the  $(L_s+j)$ -th block rows of  $\mathbf{H}_{\mathrm{TD}}^{\mathbf{s}}$ ,  $\mathbf{H}_{\mathrm{TD}}^{\mathbf{svcc}}$ ,  $\mathbf{H}_{\mathrm{TD}}^{\mathbf{c}}$ , and  $\mathbf{H}_{\mathrm{TD}}^{\mathbf{sccv}}$  in Fig. 7.

2) Secondly, extra channel codeword sequences  $v_{L_s+m_0}$ ,  $v_{L_s+m_0+1}$ ,  $\cdots$ ,  $v_{L_c}$  (consisting of mainly parity-check bits) are derived based on the remaining part of  $\mathbf{H}_{\mathrm{TD}}^{\mathrm{c}}$  shown in the black dashed frame of Fig. 7, i.e.,  $\mathbf{H}_{\mathrm{remaining}}$ . We define  $L_{\mathrm{extra}}$  as the number of block columns added after the block column corresponding to  $v_{L_s+m_0-1}$  (i.e. after the  $(L_s+m_0)$ -th block column of  $\mathbf{H}_{\mathrm{TD}}^{\mathrm{c}}$ ). To ensure that encoding could be performed based on  $\mathbf{H}_{\mathrm{remaining}}$  and the known  $v_{L_s+m_0-m_1}, v_{L_s+m_0-m_1+1}, \cdots, v_{L_s+m_0-1}$ , the number of parity-check equations in  $\mathbf{H}_{\mathrm{remaining}}$  should be no more than the number of variable nodes in  $v_{L_s+m_0}, v_{L_s+m_0+1}, \cdots, v_{L_c-1}$ , i.e.,

$$m_c(L_{\text{extra}} + m_1) - m_{\text{all-zero}} \le n_c L_{\text{extra}},$$
 (24)

where  $m_{\rm all-zero}$  denotes the number of all-zero block rows in  ${\bf B}_{\rm remaining}$ , which denotes the remaining part of  ${\bf B}_{\rm TD}^{\rm c}$  shown in the black dashed frame of Fig. 7. In other words,  $L_{\rm extra}$  should be the smallest integer selected such that (24) is satisfied. Finally, we can calculate the channel coupling length using  $L_c = L_s + m_0 + L_{\rm extra}$ .

TABLE IV Channel thresholds and source thresholds of different codes at  $p_1=0.01$ . The Shannon limit equals  $-12.02~\mathrm{dB}$ .

Code $\mathbf{B}_{\mathrm{TD}_{11}}^{0.01}$		$\mathbf{B}_{\mathrm{T}}^{0}$		$\mathbf{B}_{\mathrm{T}}^{0.}$		$\mathbf{B}_{\mathrm{T}}^{0}$		$\mathbf{B}_{\mathrm{J}_{\mathrm{new}}~0.01}^{\mathrm{opt2}}$	$\mathbf{B}_{\mathrm{TDn}\epsilon}^{0.01}$	[30]	
w	6	8	6	8	6	8	6	8	None	6	8
$(E_s/N_0)_{\rm th}$ (dB)	-9.999	-10.795	-11.087	-11.112	-10.646	-10.850	-11.104	-11.153	-10.170	-11.022	-11.112
$p_{ m th}$	0.045	0.046	0.045	0.046	0.091	0.095	0.091	0.095	0.084	0.031	0.032

#### B. Sliding window-based decoder and threshold analysis

We apply a sliding window-based joint BP algorithm to decode the proposed SC-JSCCs and use w to denote the window size. As the blue dashed frames shown in Fig. 7, w block rows and block columns of  $\mathbf{H}_{\mathrm{TD}}^{\mathrm{s}}$ ,  $\mathbf{H}_{\mathrm{TD}}^{\mathrm{c}}$ ,  $\mathbf{H}_{\mathrm{TD}}^{\mathrm{ccv}}$ , and  $\mathbf{H}_{\mathrm{TD}}^{\mathrm{svec}}$  are included in a window. We can regard the protomatrix in a window as a JSC-BC and use the joint BP algorithm in [21] to decode the first  $n_s z$  source symbols in the window, which are defined as the target symbols. In the next decoding timeslot, the window will slide to the right and downward, i.e., moving from the blue dashed frames to the red dashed frames in Fig. 7, and so on. Moreover, all updated log-likelihood ratio (LLR) messages and previously decoded source symbols and channel codewords would be used to facilitate decoding the source symbols and channel codewords in the current window.

The decoding differs slightly from previous decoders when the last window is reached. The last window contains the last w block columns and their connected rows of the source SC-DP-LDPC parity-check matrix (i.e., the last  $w + m_0$  source block rows), the last  $w + m_0$  block columns and their connected rows of the SC-SCCV linking parity-check matrix (i.e., the last  $w + m_0$  SC-SCCV block rows), the last  $w + m_0 + L_{\text{extra}}$ block columns and their connected rows of the channel SC-DP-LDPC parity-check matrix, and the last w block columns and their connected rows of the SC-SVCC linking paritycheck matrix (i.e., the last  $w + m_3$  SC-SVCC block rows). For example, if we assume  $m_0 = m_1 = m_2 = m_3 = 1$  and w=3 and the decoding of the second to last window has been completed, which means  $s_{L_s-4}$  has been decoded based on sub-protomatrices in the blue frames shown in Fig. 8. Next, blue frames slide to the right and downward to the last window, denoted by red frames in Fig. 8. The red frames include all remaining sub-protomatrices.

Using the joint BP algorithm, we decode all the source symbols in the last window. Also, decoding in the last window can be facilitated by previously decoded source symbols, channel codewords, and some messages updated in the previous window.

As mentioned above, we can regard the protomatrix in a window (w block rows and block columns of  $\mathbf{B}_{\mathrm{TD}}^{\mathrm{s}}$ ,  $\mathbf{B}_{\mathrm{TD}}^{\mathrm{c}}$ ,  $\mathbf{B}_{\mathrm{TD}}^{\mathrm{c}}$ , and  $\mathbf{B}_{\mathrm{TD}}^{\mathrm{scc}}$  in the blue dashed frames in Fig. 7) as a JSC-BC. We therefore can use algorithms for calculating the channel and source thresholds of a JSC-BC to calculate the channel and source thresholds of a SC-JSCC, i.e., the JP-EXIT algorithm [17] and UP-EXIT algorithm, respectively. When the MI between the APP-LLR of the first  $n_s$  VNs in a window and their corresponding symbols reaches "1" or the maximum number of iterations is reached, the algorithms will stop.

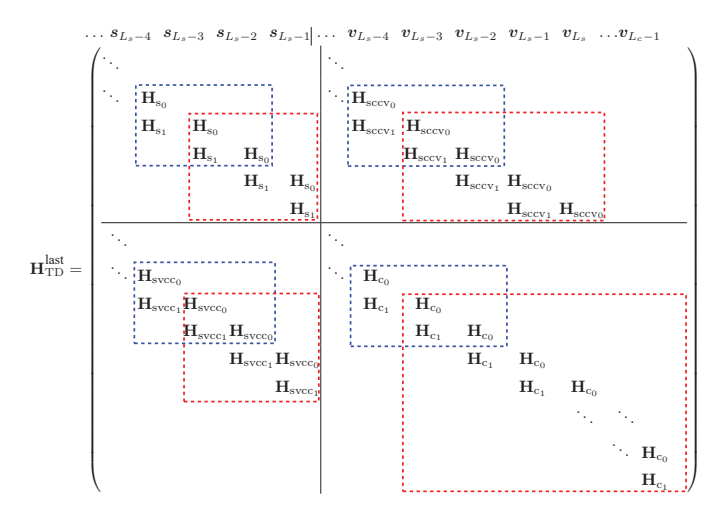


Fig. 8. The last decoding window is specified by the red frames when  $m_0=m_1=m_2=m_3=1$  and w=3.

#### C. Results and discussions

In this section, we construct some SC-JSCCs from JSC-BCs using the differential evolution (DE) algorithm [13]. When calculating the thresholds for SC-JSCCs, JSC-BCs, and SC-DP-LDPC codes [30], we set the maximum number of iterations to 200.

When simulating the SSER performance of SC-JSCCs and JSC-BCs, we assume that both decoders have the same decoding latency, i.e., both the block decoder and the window decoder need to receive the same number of channel inputs before starting the decoding process [29]. We set the maximum number of iterations for JSC-BCs to 200 while using the syndrome checking to terminate the iteration early. In the decoding of SC-JSCCs and SC-DP-LDPC codes, the iterations will not be stopped until the maximum number of iterations is reached. Thus, we set the maximum number of iterations to 100 for SC-JSCCs and SC-DP-LDPC codes in order to reduce the simulation time. Note that adjusting the maximum number of iterations from 100 to 200 for SC-JSCCs and SC-DP-LDPC codes may result in improved error performance compared to the simulation results presented in this section.

1) Low-entropy sources: We design some SC-JSCCs for low-entropy sources.

Example #4: When  $p_1=0.01$ , we first construct a SC-JSCC based on  $\mathbf{B}_{\mathrm{J}_{\mathrm{new}_0.01}}^{\mathrm{opt}\,1}$  in (12). We start by setting  $m_0=m_1=m_3=1$  and  $m_2=0$ . The source SC-P-LDPC protomatrix and the channel SC-P-LDPC protomatrix are to be the same as the SC-DP-LDPC code  $\mathbf{B}_{\mathrm{TD}_{\mathrm{new}}}^{0.01}$  in [30], which are obtained

based on  ${\bf B}_{\rm J3~opt3}^{0.01}$  in (12). We thus obtain

$$\begin{aligned} \mathbf{B}_{s_{1}}^{0,01} &= \begin{pmatrix} 0\ 0\ 0\ 1\ 1\ 0\ 2\ 1 \\ 0\ 0\ 0\ 1\ 1\ 1\ 0\ 1 \end{pmatrix}; \ \mathbf{B}_{s_{0}}^{0,01} &= \begin{pmatrix} 1\ 1\ 2\ 0\ 2\ 1\ 1\ 0 \\ 1\ 2\ 1\ 1\ 0\ 1\ 1\ 1 \end{pmatrix}; \\ \mathbf{B}_{c_{1}}^{0,01} &= \begin{pmatrix} 0\ 0\ 0\ 0\ 0 \\ 1\ 1\ 0\ 0\ 1 \\ 2\ 0\ 0\ 1\ 0 \end{pmatrix}; \ \mathbf{B}_{c_{0}}^{0,01} &= \begin{pmatrix} 3\ 0\ 1\ 0\ 0 \\ 0\ 1\ 0\ 1\ 0 \\ 0\ 1\ 0\ 0\ 1 \end{pmatrix}; \ \mathbf{B}_{sccv_{0}}^{0,01} &= \begin{pmatrix} 1\ 0\ 0\ 0\ 0 \\ 3\ 1\ 0\ 0\ 0 \end{pmatrix}; \\ \mathbf{B}_{svcc_{1}}^{0,01} &= \begin{pmatrix} 0\ 0\ 0\ 0\ 2\ 0\ 1\ 0 \\ 0\ 0\ 0\ 0\ 0\ 0\ 0\ 0 \end{pmatrix}; \ \mathbf{B}_{svcc_{0}}^{0,01} &= \begin{pmatrix} 0\ 0\ 0\ 0\ 1\ 0\ 2\ 0 \\ 0\ 0\ 0\ 0\ 0\ 0\ 0\ 0 \end{pmatrix}; \end{aligned}$$

and we denote the corresponding SC-JSCC by  ${\bf B}_{{\rm TD}_{11}}^{0.01}.$  Next, we set  $m_2 = 1$  and use the DE algorithm to construct the SC-SCCV sub-protomatrices based on  $\mathbf{B}_{s_i}^{0.01}$ ,  $\mathbf{B}_{c_i}^{0.01}$ , and  $\mathbf{B}_{\text{svc}_i}^{0.01}$ (i = 0, 1) shown in (25) to form a new SC-JSCC. We set the maximum row weight of the SC-JSCC no larger than that of  $B_{\mathrm{J}_{\mathrm{new}\_0.01}}^{\mathrm{opt1}}$  to control the decoding complexity. The SC-SCCV linking sub-protomatrices obtained are

$$\mathbf{B}_{\text{sccv}_{1}'}^{0.01} = \begin{pmatrix} 1 & 0 & 0 & 0 & 0 \\ 0 & 0 & 0 & 1 \end{pmatrix}; \ \mathbf{B}_{\text{sccv}_{0}'}^{0.01} = \begin{pmatrix} 1 & 0 & 0 & 0 & 0 \\ 2 & 1 & 0 & 0 & 0 \end{pmatrix}$$
(26)

and the corresponding SC-JSCC is denoted as  ${\bf B}_{{\rm TD}_{12}}^{0.01}$ .

Secondly, we start by setting  $m_0 = m_1 = m_3 = 1$  and  $m_2=0$ , and construct source sub-protomatrices  ${f B}_{
m so}^{0.01}$  and  $\mathbf{B}_{\mathrm{s}_{1}}^{0.01}$ , channel sub-protomatrices  $\mathbf{B}_{\mathrm{c}_{0}}^{0.01}$  and  $\mathbf{B}_{\mathrm{c}_{1}}^{0.01}$ , and SC-SVCC sub-protomatrices  $\mathbf{B}_{\mathrm{svcc}_{0}}^{0.01}$  and  $\mathbf{B}_{\mathrm{svcc}_{1}}^{0.01}$  based on the JSC-BC  $\mathbf{B}_{\mathrm{J}_{\mathrm{new}}_{0.01}}^{\mathrm{opt2}}$  (14). We obtain

and we denote the corresponding SC-JSCC as  $B_{TD_{21}}^{0.01}$ .

Then, we set  $m_2 = 1$  and use the DE algorithm to construct the SC-SCCV sub-protomatrices based on  $\mathbf{B}_{s_i}^{0.01}$ ,  $\mathbf{B}_{c_i}^{0.01}$ , and  $\mathbf{B}_{\mathrm{svcc}_{i}}^{0.01}$  (i=0,1) shown in (27) to form a new SC-JSCC. We set the maximum row weight of the SC-JSCC no larger than that of  $B_{J_{\rm new\_0.01}}^{\rm opt2}$  to control the decoding complexity. The SC-SCCV linking sub-protomatrices obtained are

$$\mathbf{B}_{\text{sccv}_1}^{0.01} = \begin{pmatrix} 1 & 0 & 0 & 0 & 0 \\ 0 & 0 & 0 & 1 & 0 \end{pmatrix}; \ \mathbf{B}_{\text{sccv}_0}^{0.01} = \begin{pmatrix} 1 & 0 & 0 & 0 & 0 \\ 2 & 1 & 0 & 0 & 0 \end{pmatrix}$$
 (28)

and the corresponding SC-JSCC code is denoted as  ${\bf B}_{{\rm TD}_{22}}^{0.01}$ .

Table IV lists the source thresholds and channel thresholds of the new SC-JSCCs,  $\mathbf{B}_{\mathrm{Jnew},0}^{\mathrm{opt2}}$  (with best error performance among block codes), and  $\mathbf{B}_{\mathrm{TD}_{\mathrm{new}}}^{\mathrm{opt0},01}$  [30]. We have the following observations: i) The channel thresholds of Type-II SC-JSCCs, namely  $B_{\mathrm{TD}_{12}}^{0.01}$  and  $B_{\mathrm{TD}_{22}}^{0.01}$  differ within 0.05 dB between window size  $\overline{w} = 6$  and  $\overline{w} = 8$ ; ii) The channel thresholds of Type-I SC-JSCCs, i.e.,  $\mathbf{B}_{\mathrm{TD}_{11}}^{0.01}$  and  $\mathbf{B}_{\mathrm{TD}_{21}}^{0.01}$ , as well as the SC-DP-LDPC code  $\mathbf{B}_{\mathrm{TD}_{\mathrm{new}}}^{0.01}$  [30], exhibit a larger difference between window size w=6 and w=8, ranging from 0.09 dB to 0.8 dB; iii)  $\mathbf{B}_{\mathrm{TD}_{22}}^{0.01}$  at w=8 has a channel threshold of  $0.041~\mathrm{dB}$  lower than  $\mathbf{B}_{\mathrm{TD}_{\mathrm{new}}}^{0.01}$  at w=8; iv) All SC-JSCCs with w = 8 have lower channel thresholds than the JSC-BC code  ${f B}_{J_{\rm new\_0.01}}^{\rm opt2};$  v)  ${f B}_{{
m TD}_{21}}^{0.01}$  and  ${f B}_{{
m TD}_{22}}^{0.01}$  have the highest source thresholds among these codes.

Fig. 9 shows the SSER performance of the SC-JSCCs and the SC-DP-LDPC code  $\mathbf{B}_{\mathrm{TD}_{\mathrm{new}}}^{0.01}$  when w=6 and w=8. For w = 8, we set  $z = 4 \times 50 = 200$ . For w = 6, we set  $z = 4 \times 67 = 268$ . w and z are set to maintain a similar code length in each window and to achieve a similar decoding latency as the JSC-BC  ${\bf B}_{\rm J_{new\_0.01}}^{\rm opt2}$ . Fig. 9 also presents the SSER performance of  ${\bf B}_{\rm J_{new\_0.01}}^{\rm opt2}$  for comparison. We have the following observations.

- i) Type-I SC-JSCCs, i.e.,  $\mathbf{B}_{\mathrm{TD}_{11}}^{0.01}$  and  $\mathbf{B}_{\mathrm{TD}_{21}}^{0.01}$ , as well as the SC-DP-LDPC code  $\mathbf{B}_{\mathrm{TD}_{\mathrm{new}}}^{0.01}$  [30] with w=8 have better error performance than that with w=6. Their channel thresholds with w = 8 are lower than those with w = 6. Type-II SC-JSCCs, namely  ${\bf B}_{{\rm TD}_{12}}^{0.01}$  and  ${\bf B}_{{\rm TD}_{22}}^{0.01}$  at w=6have better error performance than those at w = 8. Their channel thresholds at w = 6 and w = 8 are very close. Additionally, the lifting factor at w = 6 is larger than that at w = 8. This suggests that the performance difference is not solely dependent on the channel threshold and indicates the importance of considering the lifting factor along with the channel threshold for a given window size so as to achieve good error performance in scenarios where the code lengths are similar within a window.
- ii) Type-II SC-JSCCs, i.e.,  $\mathbf{B}_{\mathrm{TD}_{12}}^{0.01}$  and  $\mathbf{B}_{\mathrm{TD}_{n2}}^{0.01}$  at w=6 have better error performance than  $\mathbf{B}_{\mathrm{TD}_{new}}^{0.01}$  at w=6 and w=8 and the JSC-BC  $\mathbf{B}_{\mathrm{J}_{new}_{-0.01}}^{\mathrm{opt2}}$  when  $E_s/N_0$  is large. iii)  $\mathbf{B}_{\mathrm{TD}_{22}}^{0.01}$  at w=6 has the best error performance among
- all codes.
- iv) All codes do not suffer from an error floor caused by the source compression because of their large source thresholds relative to  $p_1 = 0.01$ .
- Table IV shows that except for  ${\bf B}_{{\rm TD}_{11}}^{0.01}$  at w=6, other SC-JSCCs designed at  $p_1 = 0.01$  have lower channel thresholds than  $\mathbf{B}_{J_{\text{new\_0.01}}}^{\text{opt2}}$ . Fig. 9 shows  $\mathbf{B}_{J_{\text{new\_0.01}}}^{\text{opt2}}$  has better SSER performance than  $\mathbf{B}_{\text{TD}_{11}}^{0.01}$  with w = 6. However, other SC-JSCCs achieve similar or even worse error performance than  ${\bf B}_{\rm J_{new\_0.01}}^{\rm opt2}$  in low  $E_s/N_0$  region although they have better theoretical channel thresholds. One of the reasons for this phenomenon is that error propagation has been observed in the SSER simulation results of SC-JSCCs, especially in the low  $E_s/N_0$  region where the probability of error occurrence increases significantly. Once an error occurs, it will propagate to and cause errors in subsequent time slots. Error propagation will degrade the performance of SC-JSCCs. Unlike SC-JSCCs, JSC-BCs are not affected by error propagation. Moreover, in addition to the window size w, the lifting factor z also affects the error performance of SC-JSCCs. In Fig. 9, the lifting factor value of JSC-BC is w times that of SC-JSCCs. The error performance of SC-JSCCs is collectively influenced by factors such as w, error propagation, and z.

Example #5: When  $p_1 = 0.04$ , we first construct a SC-JSCC based on  $\mathbf{B}_{\mathrm{J}_{\mathrm{new}},0.04}^{\mathrm{opt1}}$  (15). We begin by setting  $m_0=m_1=$ 

TABLE V Channel thresholds and source thresholds of different codes at  $p_1=0.04$ . The Shannon limit equals  $-7.00~\mathrm{dB}$ .

Code	Code $\mathbf{B}_{\mathrm{TD}_{11}}^{0.04}$		D <sub>mp</sub> D <sub>mp</sub>		${f B}_{{ m TD}_{21}}^{0.04}$		${f B}_{{ m TD}_{22}}^{0.04}$		$\mathbf{B}_{\mathrm{J}_{\mathrm{new}}\ 0.04}^{\mathrm{opt2}}$ $\mathbf{B}_{\mathrm{TD}_{\mathrm{new}}}^{0.04}$		ew [30]
w	6	8	6	8	6	8	6	8	None	6	8
$(E_s/N_0)_{\rm th}$ (dB)	-5.386	-6.120	-6.390	-6.430	-5.547	-6.365	-6.442	-6.476	-5.880	-6.311	-6.441
$p_{ m th}$	0.129	0.150	0.129	0.150	0.394	0.394	0.394	0.394	0.217	0.084	0.091

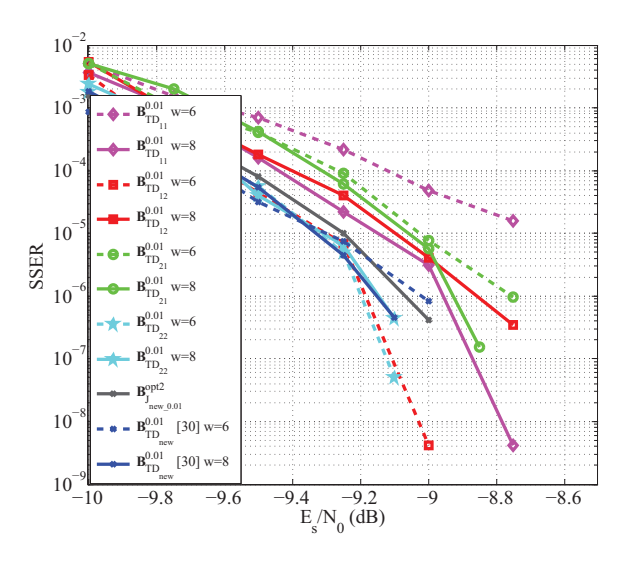


Fig. 9. SSER performance comparison between new SC-JSCCs,  $\mathbf{B}_{\mathrm{Jnew}}^{\mathrm{opt2}}$  and SC-DP-LDPC codes at  $p_1=0.01$ . The lifting factors for SC-JSCCs are  $z=z_1z_2=4\times67=268$  and  $z=z_1z_2=4\times50=200$  when w=6 and w=8, respectively.  $L_s=128$  and  $L_c=130$ .  $R_{\mathrm{TD}}=1.969$  for SC-JSCCs.

 $m_3=1$  and  $m_2=0$ . The source SC-P-LDPC protomatrix and the channel SC-P-LDPC protomatrix are set to be the same as the SC-DP-LDPC code  ${\bf B}_{{
m TD}_{
m new}}^{0.04}$  in [30], which are obtained based on  ${\bf B}_{{
m J}_{
m opt1}}^{0.04}$  (15). We thus obtain

and the corresponding SC-JSCC is denoted as  $\mathbf{B}_{\mathrm{TD}_{11}}^{0.04}$ . Next, we set  $m_2=1$  and use the DE algorithm to construct the SC-SCCV sub-protomatrices based on  $\mathbf{B}_{s_i}^{0.04}$ ,  $\mathbf{B}_{s_i}^{0.04}$ , and  $\mathbf{B}_{\mathrm{svec}_i}^{0.04}$  (i=0,1) shown in (29) to form a new SC-JSCC. We set the maximum row weight of the SC-JSCC no larger than that of  $\mathbf{B}_{\mathrm{Jopt\_new1}}^{0.04}$  to maintain the same decoding complexity as  $\mathbf{B}_{\mathrm{Jopt\_new1}}^{0.04}$ . The SC-SCCV linking sub-protomatrices obtained are

$$\mathbf{B}_{\text{sccv}_{1}^{'}}^{0.04} = \begin{pmatrix} 1 & 0 & 0 & 0 & 1 \\ 0 & 0 & 0 & 0 & 0 \end{pmatrix}; \ \mathbf{B}_{\text{sccv}_{0}^{'}}^{0.04} = \begin{pmatrix} 1 & 0 & 0 & 0 & 0 \\ 1 & 1 & 0 & 0 & 0 \end{pmatrix}. \tag{30}$$

and the corresponding SC-JSCC code is denoted as  $\mathbf{B}_{\mathrm{TD}_{12}}^{0.04}$ . Secondly, we begin by setting  $m_0 = m_1 = m_3 = 1$  and  $m_2 = 0$ , and construct source sub-protomatrices  $\mathbf{B}_{\mathrm{so}}^{0.04}$  and

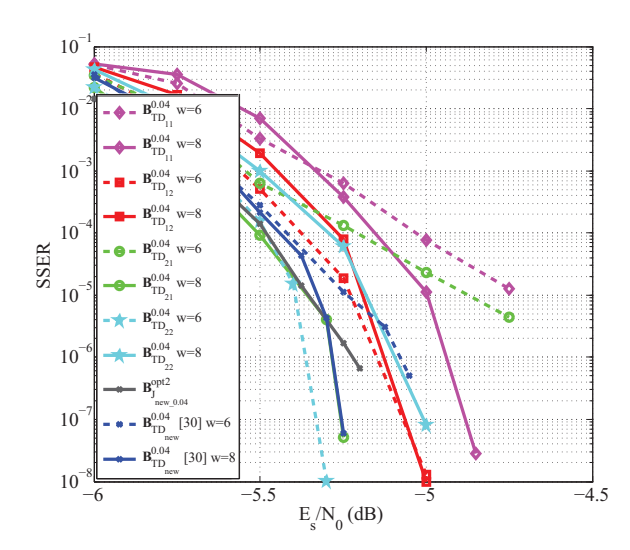


Fig. 10. SSER performance comparison between new SC-JSCCs,  $\mathbf{B}_{\mathrm{J_{new}},0.04}^{\mathrm{opt}\,2}$  and SC-DP-LDPC codes at  $p_1=0.04$ . The lifting factors for SC-JSCCs are  $z=z_1z_2=4\times134=536$  and  $z=z_1z_2=4\times100=400$  when w=6 and w=8, respectively.  $L_s=128$  and  $L_c=130$ .  $R_{\mathrm{TD}}=0.985$  for SC-JSCCs.

 $\mathbf{B}_{s_1}^{0.04},$  channel sub-protomatrices  $\mathbf{B}_{c_0}^{0.04}$  and  $\mathbf{B}_{c_1}^{0.04},$  and SC-SVCC sub-protomatrices  $\mathbf{B}_{svcc_0}^{0.04}$  and  $\mathbf{B}_{svcc_1}^{0.04}$  based on the JSC-BC  $\mathbf{B}_{J_{new\_0.04}}^{opt2}$  (17). We obtain

$$\mathbf{B}_{s_{1}}^{0.04} = \begin{pmatrix} 0 & 0 & 1 & 2 \\ 0 & 0 & 0 & 1 \end{pmatrix}; \mathbf{B}_{s_{0}}^{0.04} = \begin{pmatrix} 1 & 0 & 1 & 1 \\ 1 & 1 & 1 & 0 \end{pmatrix}; \mathbf{B}_{sccv_{0}}^{0.04} = \begin{pmatrix} 1 & 0 & 0 & 0 & 0 \\ 3 & 1 & 0 & 0 & 0 \end{pmatrix}; 
\mathbf{B}_{c_{1}}^{0.04} = \begin{pmatrix} 0 & 0 & 0 & 0 & 0 \\ 1 & 0 & 0 & 0 & 1 \\ 1 & 0 & 0 & 1 & 0 \end{pmatrix}; \mathbf{B}_{c_{0}}^{0.04} = \begin{pmatrix} 3 & 0 & 1 & 0 & 0 \\ 2 & 0 & 0 & 1 & 0 \\ 0 & 1 & 0 & 1 & 1 \end{pmatrix}; 
\mathbf{B}_{svcc_{1}}^{0.04} = \begin{pmatrix} 0 & 0 & 0 & 1 \\ 0 & 0 & 0 & 0 \\ 0 & 0 & 0 & 0 \end{pmatrix}; \mathbf{B}_{svcc_{0}}^{0.04} = \begin{pmatrix} 0 & 0 & 0 & 0 \\ 0 & 0 & 0 & 0 \\ 0 & 2 & 0 & 0 \end{pmatrix};$$
(31)

and we denote the corresponding SC-JSCC as  ${\bf B}_{{\rm TD}_{21}}^{0.04}$ .

Next, we set  $m_2=1$  and use the DE algorithm to construct the SC-SCCV sub-protomatrices based on  $\mathbf{B}_{\mathrm{s}_i}^{0.04}$ ,  $\mathbf{B}_{\mathrm{c}_i}^{0.04}$ , and  $\mathbf{B}_{\mathrm{svcc}_i}^{0.04}$  (i=0,1) shown in (31) to form a new SC-JSCC. We set the maximum row weight of the SC-JSCC no larger than that of  $\mathbf{B}_{\mathrm{J_{new}}_{0.04}}^{\mathrm{opt2}}$  to maintain the same decoding complexity as  $\mathbf{B}_{\mathrm{J_{new}}_{0.04}}^{\mathrm{opt2}}$ . The SC-SCCV linking sub-protomatrices obtained are

$$\mathbf{B}_{\text{sccv}_1}^{0.04} = \begin{pmatrix} 1 & 0 & 0 & 0 & 0 \\ 1 & 0 & 0 & 0 & 1 \end{pmatrix}; \ \mathbf{B}_{\text{sccv}_0}^{0.04} = \begin{pmatrix} 1 & 0 & 0 & 0 & 0 \\ 1 & 1 & 0 & 0 & 0 \end{pmatrix}$$
(32)

and the corresponding SC-JSCC code is denoted as  $B_{\mathrm{TD}_{22}}^{0.04}$ .

Table V lists the source thresholds and channel thresholds of the new SC-JSCCs,  $\mathbf{B}_{\mathrm{J}_{\mathrm{new},0.04}}^{\mathrm{opt2}}$  (with best error performance among block codes), and  $\mathbf{B}_{\mathrm{TD}_{\mathrm{new}}}^{\mathrm{or},0.04}$  [30]. We have the following observations: i) The thresholds of Type-II SC-JSCCs, namely

-2.595

0.171

0.259 (w = 6)

0.318(w = 6)

2.995 (w = 8)

0.434 (w = 8)

TABLE VI Channel thresholds and source thresholds of different codes at  $p_1=0.10$  and  $p_1=0.20$ .

 $\mathbf{B}_{\mathrm{TD}_{12}}^{0.04}$  and  $\mathbf{B}_{\mathrm{TD}_{22}}^{0.04}$ , only differ within 0.04 dB between window size w=6 and w=8. Type-I SC-JSCCs, i.e.,  $\mathbf{B}_{\mathrm{TD}_{11}}^{0.04}$  and  $\mathbf{B}_{\mathrm{TD}_{21}}^{0.04}$ , as well as the SC-DP-LDPC code  $\mathbf{B}_{\mathrm{TD}_{\mathrm{new}}}^{0.04}$  [30], exhibit a larger difference in their channel thresholds between window size w=6 and w=8, ranging from around 0.10 dB to 0.80 dB. This phenomenon is also observed in Table IV; ii)  $\mathbf{B}_{\mathrm{TD}_{22}}^{0.04}$  at w=8 has a channel threshold of 0.035 dB lower than  $\mathbf{B}_{\mathrm{TD}_{\mathrm{new}}}^{0.04}$  at w=8; iii) All SC-JSCCs with w=8 have lower channel thresholds than the JSC-BC code  $\mathbf{B}_{\mathrm{Jnew}_{-0.04}}^{\mathrm{opt2}}$ ; iv)  $\mathbf{B}_{\mathrm{TD}_{21}}^{0.04}$  and  $\mathbf{B}_{\mathrm{TD}_{22}}^{0.04}$  have the highest source thresholds among these codes.

 $(E_s/N_0)_{\rm th}$  (dB)

-2.958 (w = 6)

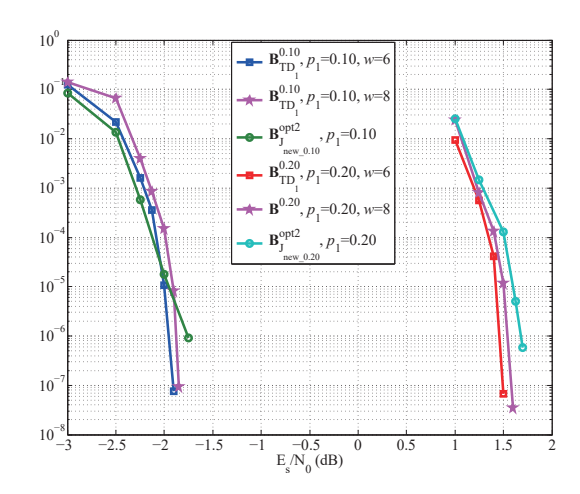
0.434 (w = 6)

Fig. 10 shows the SSER performance of the SC-JSCCs and the SC-DP-LDPC code  ${\bf B}_{{\rm TD}_{\rm new}}^{0.04}$  when w=6 and w=8. For w=8, we set  $z=4\times 100=400$ . For w=6, we set  $z=4\times 134=536$ . Fig. 10 also presents the SSER performance of  ${\bf B}_{{\rm J}_{\rm new},0.04}^{\rm opt2}$  for comparison. We can observe the followings: a) Type-I SC-JSCCs, i.e.,  ${\bf B}_{{\rm TD}_{\rm new}}^{0.04}$  and  ${\bf B}_{{\rm TD}_{\rm 21}}^{0.04}$ , as well as the SC-DP-LDPC code  ${\bf B}_{{\rm TD}_{\rm new}}^{0.04}$  [30] with w=8 have better error performance than that with w=6. Their channel thresholds at w=8 are lower than those at w=6. Type-II SC-JSCCs, namely  ${\bf B}_{{\rm TD}_{\rm 12}}^{0.04}$  and  ${\bf B}_{{\rm TD}_{\rm 22}}^{0.04}$  at w=6 have better error performance than that at w=8. Their channel thresholds at w=6 and w=8 are very close; b)  ${\bf B}_{{\rm TD}_{\rm 22}}^{0.04}$  at w=6 has the best error performance among those codes; c) No error floor is observed due to the large source thresholds of these codes relative to  $p_1=0.04$ .

2) High-entropy sources: We design some SC-JSCCs for high-entropy sources. Based on the observations above, we can conclude that Type-II SC-JSCCs constructed based on the optimized JSC-BCs, i.e.,  $\mathbf{B}_{\mathrm{TD}_{22}}^{0.01}$  and  $\mathbf{B}_{\mathrm{TD}_{22}}^{0.04}$ , possess excellent theoretical thresholds and simulated SSER results at w=6. Therefore in the following, we construct only Type-II SC-JSCCs based on the optimized JSC-BCs.

Example #6: When  $p_1=0.10$ , we consider  $\mathbf{B}_{\mathrm{J_{new},0.10}}^{\mathrm{opt2}}$  in (19). We set  $m_0=m_1=m_2=m_3=1$  and construct source sub-protomatrices  $\mathbf{B}_{\mathrm{s_0}}^{0.10}$  and  $\mathbf{B}_{\mathrm{s_1}}^{0.10}$ , channel sub-protomatrices  $\mathbf{B}_{\mathrm{c_0}}^{0.10}$  and  $\mathbf{B}_{\mathrm{c_1}}^{0.10}$ , SC-SVCC sub-protomatrices  $\mathbf{B}_{\mathrm{svec_0}}^{0.10}$  and  $\mathbf{B}_{\mathrm{svec_1}}^{0.10}$ , and SC-SCCV sub-protomatrices  $\mathbf{B}_{\mathrm{sccv_0}}^{0.10}$  and  $\mathbf{B}_{\mathrm{sccv_1}}^{0.10}$ , and we obtain

$$\mathbf{B}_{s_{1}}^{0.10} = \begin{pmatrix} 0 & 0 & 2 & 0 \\ 1 & 0 & 0 & 0 \end{pmatrix}; \, \mathbf{B}_{s_{0}}^{0.10} = \begin{pmatrix} 1 & 0 & 1 & 0 \\ 0 & 1 & 1 & 1 \end{pmatrix}; \\
\mathbf{B}_{c_{1}}^{0.10} = \begin{pmatrix} 1 & 0 & 0 & 0 & 0 \\ 1 & 0 & 0 & 0 & 1 \\ 0 & 0 & 0 & 0 & 0 \end{pmatrix}; \, \mathbf{B}_{c_{0}}^{0.10} = \begin{pmatrix} 2 & 0 & 1 & 0 & 0 \\ 1 & 0 & 0 & 1 & 0 \\ 1 & 1 & 0 & 2 & 1 \end{pmatrix}; \\
\mathbf{B}_{svcc_{1}}^{0.10} = \begin{pmatrix} 0 & 0 & 0 & 0 \\ 0 & 1 & 0 & 0 \\ 0 & 0 & 1 & 1 \end{pmatrix}; \, \mathbf{B}_{svcc_{0}}^{0.10} = \begin{pmatrix} 0 & 0 & 0 & 0 \\ 0 & 1 & 0 & 1 \\ 0 & 0 & 1 & 0 \end{pmatrix}; \\
\mathbf{B}_{sccv_{1}}^{0.10} = \begin{pmatrix} 0 & 1 & 0 & 0 & 0 \\ 0 & 0 & 0 & 0 & 0 \end{pmatrix}; \, \mathbf{B}_{sccv_{0}}^{0.10} = \begin{pmatrix} 1 & 0 & 0 & 0 & 0 \\ 2 & 1 & 0 & 0 & 0 \\ 2 & 1 & 0 & 0 & 0 \end{pmatrix}.$$
(33)



0.209 (w = 8)

0.318(w = 8)

0.831

0.288

Fig. 11. SSER performance comparison between new SC-JSCCs and new JSC-BC codes at  $p_1=0.10$  and  $p_1=0.20$ . The lifting factors for SC-JSCCs are  $z=z_1z_2=4\times134=536$  and  $z=z_1z_2=4\times100=400$  when w=6 and w=8, respectively.  $L_s=128$  and  $L_c=130$ .  $R_{\rm TD}=0.985$  for SC-JSCCs.

We denote the corresponding SC-JSCC as  ${\bf B}_{{
m TD}_1}^{0.10}.$ 

When  $p_1=0.20$ , we consider  $\mathbf{B}_{\mathrm{J}_{\mathrm{new},0.20}}^{\mathrm{opt}2}$  in (19). We also set  $m_0=m_1=m_2=m_3=1$ , and construct source sub-protomatrices  $\mathbf{B}_{\mathrm{s}_0}^{0.20}$  and  $\mathbf{B}_{\mathrm{s}_1}^{0.20}$ , channel sub-protomatrices  $\mathbf{B}_{\mathrm{c}_0}^{0.20}$  and  $\mathbf{B}_{\mathrm{c}_1}^{0.20}$ , SC-SVCC sub-protomatrices  $\mathbf{B}_{\mathrm{svcc}_0}^{0.20}$  and  $\mathbf{B}_{\mathrm{svcc}_1}^{0.20}$ , and SC-SCCV sub-protomatrices  $\mathbf{B}_{\mathrm{sccv}_0}^{0.20}$  and  $\mathbf{B}_{\mathrm{sccv}_1}^{0.20}$ , and we obtain

$$\mathbf{B}_{s_{1}}^{0.20} = \begin{pmatrix} 0 & 0 & 1 & 0 \\ 1 & 0 & 1 & 0 \end{pmatrix}; \mathbf{B}_{s_{0}}^{0.20} = \begin{pmatrix} 1 & 0 & 1 & 1 \\ 0 & 1 & 0 & 0 \end{pmatrix}; 
\mathbf{B}_{c_{1}}^{0.20} = \begin{pmatrix} 0 & 0 & 0 & 0 & 0 \\ 0 & 0 & 0 & 1 & 1 \\ 2 & 0 & 0 & 0 & 0 \end{pmatrix}; \mathbf{B}_{c_{0}}^{0.20} = \begin{pmatrix} 3 & 0 & 1 & 0 & 0 \\ 1 & 0 & 0 & 1 & 0 \\ 0 & 1 & 0 & 1 & 1 \end{pmatrix}; 
\mathbf{B}_{svcc_{1}}^{0.20} = \begin{pmatrix} 0 & 0 & 0 & 0 \\ 0 & 0 & 0 & 1 \\ 0 & 0 & 0 & 0 \end{pmatrix}; \mathbf{B}_{svcc_{0}}^{0.20} = \begin{pmatrix} 0 & 0 & 0 & 0 \\ 0 & 0 & 0 & 0 \\ 0 & 2 & 0 & 1 \end{pmatrix}; 
\mathbf{B}_{sccv_{1}}^{0.20} = \begin{pmatrix} 0 & 0 & 0 & 0 & 0 \\ 0 & 1 & 0 & 0 & 0 \end{pmatrix}; \mathbf{B}_{sccv_{0}}^{0.20} = \begin{pmatrix} 1 & 0 & 0 & 0 & 0 \\ 2 & 1 & 0 & 0 & 0 \end{pmatrix}.$$
(34)

We denote the corresponding SC-JSCC as  $B_{TD_1}^{0.20}$ .

Table VI lists the source thresholds and channel thresholds of the new SC-JSCCs and the JSC-BCs  ${\bf B}_{\rm J_{new\_0.10}}^{\rm opt2}$  and  ${\bf B}_{\rm J_{new\_0.20}}^{\rm opt2}$ , at  $p_1=0.10$  and  $p_1=0.20$ , respectively. We can see that the SC-JSCCs have lower channel thresholds and higher source thresholds than the JSC-BCs at both  $p_1$  values.  ${\bf B}_{\rm TD_1}^{0.10}$  and  ${\bf B}_{\rm TD_1}^{0.20}$  have close channel thresholds at w=6 and w=8. When w=6, their channel thresholds lie within 0.45 dB and 0.91 dB, respectively, of the Shannon limits. Fig. 11 shows the SSER performance of  ${\bf B}_{\rm TD_1}^{0.10}$  and  ${\bf B}_{\rm TD_1}^{0.20}$  at w=6 and w=8 and the SSER performance of  ${\bf B}_{\rm TD_1}^{0.10}$  and  ${\bf B}_{\rm TD_1}^{0.20}$  and  ${\bf B}_{\rm J_{new\_0.10}}^{0.20}$ .  ${\bf B}_{\rm TD_1}^{0.10}$  and  ${\bf B}_{\rm TD_1}^{0.20}$  both have slightly

TABLE VII

Channel thresholds and source thresholds of  ${f B}_{{
m TD}_{22}}^{0.04}$  at  $p_1=0.04$  with different w values. The Shannon limit equals  $-7.00~{
m dB}$ .

w	4	6	8	10
$(E_s/N_0)_{\rm th}$ (dB)	-4.729	-6.442	-6.476	-6.479
$p_{ m th}$	0.394	0.394	0.394	0.394

#### TABLE VIII

Channel thresholds and source thresholds of  ${f B}_{{
m TD}_1}^{0.20}$  at  $p_1=0.20$  with different w values. The Shannon limit equals  $-0.65~{
m dB}$ .

w	4	6	8	10
$(E_s/N_0)_{\rm th}$ (dB)	0.999	0.259	0.209	0.200
$p_{ m th}$	0.317	0.318	0.318	0.318

better error performance with w=6 than that with w=8. They have similar error performance as the JSC-BCs in the low to medium  $E_s/N_0$  region, but outperform them in the high  $E_s/N_0$  region.

Based on the discussion of results in Fig.9 to Fig.11, we can know that both w and the lifting factor z have an impact on error performance. However, we just show results of two combinations of w and z in Fig.9 to Fig.11. To further validate the impact of w and z on error performance, we give the results of more combinations of w and z here. We take  $\mathbf{B}_{\mathrm{TD}_{22}}^{0.04}$  and  $\mathbf{B}_{\mathrm{TD}_{2}}^{0.20}$  as examples.

Table VII and Table VIII show that  $\mathbf{B}_{\mathrm{TD}2}^{0.04}$  and  $\mathbf{B}_{\mathrm{TD}1}^{0.20}$  have much lower channel thresholds with w=6, 8, and 10 than that with w=4, with the differences being at least 1.71 dB and 0.74 dB, respectively. Moreover, the differences in the channel thresholds of  $\mathbf{B}_{\mathrm{TD}2}^{0.04}$  and  $\mathbf{B}_{\mathrm{TD}1}^{0.20}$  when w=6, 8, and 10 are within 0.04 dB and 0.06 dB, respectively. Fig. 12 and Fig. 13 show the error performance for  $\mathbf{B}_{\mathrm{TD}2}^{0.04}$  and  $\mathbf{B}_{\mathrm{TD}1}^{0.20}$  with different w and z combinations, respectively. We can see that both  $\mathbf{B}_{\mathrm{TD}2}^{0.04}$  and  $\mathbf{B}_{\mathrm{TD}1}^{0.20}$  have much better error performance with w=6, 8, and 10 than that with w=4. The error performance of  $\mathbf{B}_{\mathrm{TD}2}^{0.04}$  and  $\mathbf{B}_{\mathrm{TD}1}^{0.20}$  at w=6 is better than that at w=8 and w=10. This is because the error performance is affected not only by w but also by the lifting factor. Although the channel threshold at w=6 is slightly worse than that at w=8 and w=10, the lifting factor value at w=6 is larger than that at w=8 and w=10. Therefore, considering the impact of both w and z on error performance, the simulation results are reasonable.

#### IV. CONCLUSIONS

In this paper, we first propose a joint source-channel block code (JSC-BC), whose SVCC linking base matrix is a non-zero matrix and SCCV linking base matrix consists of a zero matrix and a lower or upper triangular base matrix with "1"s on its diagonal. Next, we propose an efficient UP-EXIT algorithm, where only untransmitted VNs and their connected nodes are considered, to calculate the source threshold of a JSC-BC. For both low-entropy and high-entropy sources, we construct JSC-BCs having good source and channel thresholds. SSER simulation results show that the new JSC-BCs outperform the existing DP-LDPC codes. We also propose a

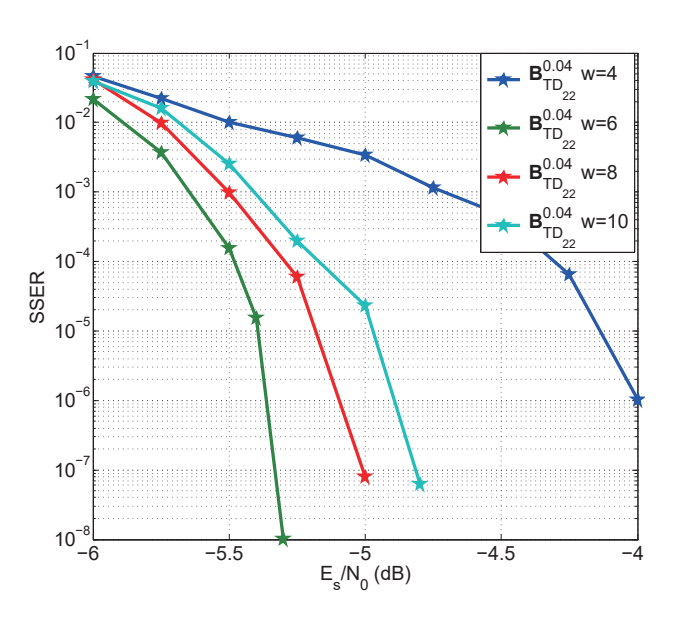


Fig. 12. SSER performance of  $\mathbf{B}_{\mathrm{TD}22}^{0.04}$  for different w and z combinations, which are  $(w=4,z=4\times200=800),~(w=6,z=4\times134=536),~(w=8,z=4\times100=400),~\mathrm{and}~(w=10,z=4\times80=320).~L_s=128,~L_c=130,~\mathrm{and}~R_{\mathrm{TD}}=0.985.$ 

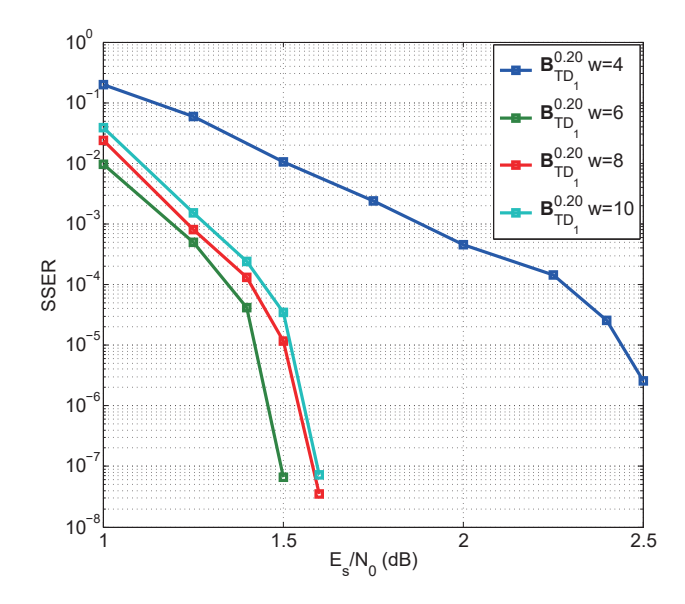


Fig. 13. SSER performance of  $\mathbf{B}_{\mathrm{TD}_{1}}^{0.20}$  for different w and z combinations, which are  $(w=4,z=4\times200=800), (w=6,z=4\times134=536), (w=8,z=4\times100=400), \text{ and } (w=10,z=4\times80=320).$   $L_{s}=128,$   $L_{c}=130,$  and  $R_{\mathrm{TD}}=0.985.$ 

new type of spatially-coupled joint source-channel code (SC-JSCC). Moreover, with 200 iterations, the channel threshold of a SC-JSCC can be as close as within 0.45 dB of the Shannon limit. Theoretical analyses and simulation results further show that the new SC-JSCCs can achieve better error performance than SC-DP-LDPCs and JSC-BCs. Since our proposed JSCC schemes can achieve good error performance for both lowentropy and high-entropy sources, we will consider applying them to multi-source transmission scenarios in the future.

#### REFERENCES

- C. Y. Bi and J. Liang, "Joint source-channel coding of JPEG 2000 image transmission over two-way multi-relay networks," *IEEE Trans. Image Process.*, vol. 26, no. 7, pp. 3594–3608, Jul. 2017.
- [2] M. G. Martini, M. Mazzotti, C. Lamy-Bergot, J. Huusko, and P. Amon, "Content adaptive network aware joint optimization of wireless video transmission," *IEEE Commun. Mag*, vol. 45, no. 1, pp. 84–90, Jan. 2007.
- [3] W. Xu, J. Hagenauer, and J. Hollmann, "Joint source-channel decoding using the residual redundancy in compressed images," in *Proc. 1996 Int. Conf. Communications*. Dallas, USA: IEEE, Jun. 1996, pp. 142–148.
- [4] J. P. Woodard and L. Hanzo, "Comparative study of turbo decoding techniques: An overview," *IEEE Trans. Veh. Technol.*, vol. 49, no. 6, pp. 2208–2233, Nov. 2000.
- [5] T. J. Richardson, M. A. Shokrollahi, and R. L. Urbanke, "Design of capacity-approaching irregular low-density parity-check codes," *IEEE Trans. Inf. Theory*, vol. 47, no. 2, pp. 619–637, Feb. 2001.
- [6] L. Guivarch, J.-C. Carlach, and P. Siohan, "Joint source-channel soft decoding of Huffman codes with turbo-codes," in *Proc. IEEE Data Compression Conf. DCC*. Snowbird, USA: IEEE, Mar. 2000, pp. 83–92.
- [7] A. Zribi, R. Pyndiah, S. Zaibi, F. Guilloud, and A. Bouallegue, "Low-complexity soft decoding of Huffman codes and iterative joint source channel decoding," *IEEE Trans. Commun.*, vol. 60, no. 6, pp. 1669–1679, June. 2012.
- [8] M. Fresia, F. Perez-Cruz, H. V. Poor, and S. Verdú, "Joint source and channel coding," *IEEE Signal Process. Mag.*, vol. 27, no. 6, pp. 104– 113, Nov. 2010.
- [9] Y. Fang, G. Bi, Y. L. Guan, and F. C. M. Lau, "A survey on protograph LDPC codes and their applications," *IEEE Commun. Surveys Tuts.*, vol. 17, no. 4, pp. 1989–2016, 4th Quart., 2015.
- [10] D. Divsalar, S. Dolinar, C. Jones, and K. Andrews, "Capacity approaching protograph codes," *IEEE J. Sel. Areas Commun.*, vol. 27, no. 6, pp. 876–888, Aug. 2009.
- [11] L. Dai, Y. Fang, Y. L. Guan, and M. Guizani, "Design of protograph LDPC-coded MIMO-VLC systems with generalized spatial modulation," *China Communications*, vol. 21, no. 3, pp. 118–136, Mar. 2024.
- [12] J. G. He, L. Wang, and P. Chen, "A joint source and channel coding scheme base on simple protograph structured codes," in *Proc. Int. Symp. Commun. Inform. Tech.*, Gold Coast, Australia, Oct. 2012, pp. 65–69.
- [13] Q. Chen, F. C. M. Lau, H. Wu, and C. Chen, "Analysis and improvement of error-floor performance for JSCC scheme based on double protograph LDPC codes," *IEEE Trans. Veh. Technol.*, vol. 69, no. 12, pp. 14316– 14329, Dec. 2020.
- [14] L. Wang, L. Xu, and S. H. Hong, "New results on radiography image transmission with unequal error protection using protograph double LDPC codes," in *Proc. Int. Symp. on Medical Information and Com*munication Technology (ISMICT), Firenze, April 2014, pp. 1–4.
- [15] J. G. He, Y. Li, and G. F. Wu, "Performance improvement of joint source-channel coding with unequal power allocation," *IEEE Wireless Commun. Lett.*, vol. 6, no. 5, pp. 582–585, 2017.
- [16] C. Chen, L. Wang, and Z. Xiong, "Matching criterion between source statistics and source coding rate," *IEEE Commun. Lett.*, vol. 19, no. 9, pp. 1504–1507, Sep. 2015.
- [17] Q. Chen, L. Wang, S. Hong, and Z. Xiong, "Performance improvement of JSCC scheme through redesigning channel code," *IEEE Commun. Lett.*, vol. 20, no. 6, pp. 1088–1091, Jun. 2016.
- [18] C. Chen, L. Wang, and F. C. M. Lau, "Joint optimization of protograph LDPC code pair for joint source and channel coding," *IEEE Trans. Commun.*, vol. 66, no. 8, pp. 3255–3267, Aug. 2018.
- [19] Q. Chen, L. Wang, S. Hong, and Y. Chen, "Integrated design of JSCC scheme based on double protograph LDPC codes system," *IEEE Commun. Lett.*, vol. 23, no. 2, pp. 218–221, Feb. 2019.
- [20] S. Hong, J. Ke, and L. Wang, "Global design of double protograph LDPC codes for joint source-channel coding," *IEEE Commun. Lett.*, vol. 27, no. 2, pp. 424–427, Feb. 2023.
- [21] S. Liu, L. Wang, J. Chen, and S. Hong, "Joint component design for the JSCC system based on DP-LDPC codes," *IEEE Trans. Commun.*, vol. 68, no. 9, pp. 5808–5818, Jun. 2020.
- [22] S. Liu, C. Chen, L. Wang, and S. Hong, "Edge connection optimization for JSCC system based on DP-LDPC codes," *IEEE Wireless Commun. Lett*, vol. 8, no. 4, pp. 996–999, Aug. 2019.
- [23] J. Zhan and F. C. M. Lau, "Joint design of source-channel codes with linear source encoding complexity and good channel thresholds based on double-protograph LDPC codes," *IEEE Commun. Lett.*, vol. 27, no. 11, pp. 2909–2913, Sep. 2023.

- [24] Q. Chen, C. Chen, Y.-C. He, and Z. Xu, "Global optimization of double protograph LDPC codes for JSCC scheme," *Science China Information Sciences*, vol. 67, no. 6, p. 169301, May 2024.
- [25] A. E. Pusane, A. J. Feltström, A. Sridharan, M. Lentmaier, K. S. Zigangirov, and J. D. J. Costello, "Implementation aspects of LDPC convolutional codes," *IEEE Trans. Commun.*, vol. 56, no. 7, pp. 1060–1069, Jul. 2008.
- [26] A. R. Iyengar, M. Papaleo, P. H. Siegel, J. K. Wolf, A. Vanelli-Coralli, and G. E. Corazza, "Windowed decoding of protograph-based LDPC convolutional codes over erasure channels," *IEEE Trans. Inf. Theory*, vol. 58, no. 4, pp. 2303–2320, Apr. 2012.
- [27] S. Kumar, A. J. Young, N. Macris, and H. D. Pfister, "Threshold saturation for spatially coupled LDPC and LDGM codes on BMS channels," *IEEE Trans. Inf. Theory*, vol. 60, no. 12, pp. 7389–7415, Dec. 2014.
- [28] K. Klaiber, S. Cammerer, L. Schmalen, and S. T. Brink, "Avoiding burst-like error patterns in windowed decoding of spatially coupled LDPC codes," in *Proc. IEEE 10th Int. Symp. Turbo Codes Iterative Inf. Process.* (ISTC). Hong Kong, China: IEEE, Dec. 2018, pp. 1–5.
- [29] A. Golmohammadi and D. G. M. Mitchell, "Concatenated spatially coupled LDPC codes with sliding window decoding for joint sourcechannel coding," *IEEE Trans. Commun.*, vol. 70, no. 2, pp. 851–864, Feb. 2021.
- [30] J. Zhan and F. C. M. Lau, "Design of joint source-channel coding scheme based on spatially-coupled DP-LDPC codes," *IEEE Commun. Lett.*, vol. 28, no. 4, pp. 749–753, Apr. 2024.
- [31] H. V. B. Neto and W. Henkel, "Multi-edge optimization of low-density parity-check codes for joint source-channel coding," in *Proc. 9th Int. ITG Conf. Syst., Commun. Coding (SCC)*, Munich, Germany, Jan. 2013, pp. 1–6.
- [32] S. Hong, Q. Chen, and L. Wang, "Performance analysis and optimization for edge connection of JSCC system based on double protograph LDPC codes," *IET Commun.*, vol. 12, no. 2, pp. 214–219, Jan. 2018.
- [33] Q. Chen, S. Hong, and Y. Chen, "Design of linking matrix in JSCC scheme based on double protograph LDPC codes," *IEEE Access*, vol. 7, pp. 92 176–92 183, July. 2019.
- [34] D. G. M. Mitchell, M. Lentmaier, and D. J. Costello, "Spatially coupled LDPC codes constructed from protographs," *IEEE Trans. Inf. Theory*, vol. 61, no. 9, pp. 4866–4889, Sep. 2015.



Jia Zhan received her PhD degree from The Hong Kong Polytechnic University, MS in communication engineering degree from Xiamen University, and BS in electronic and information engineering degree from Yantai Nanshan University in 2024, 2017 and 2013, respectively. She is currently a postdoctoral fellow at Guangdong University of Technology, Guangzhou, China. Her research interests include joint source-channel coding and coded modulation.



Wai M. Tam received BSc degree from Jinan University, China; and MPhil and PhD degrees from The Hong Kong Polytechnic University, Hong Kong SAR, China. She is currently a Research Fellow at The Hong Kong Polytechnic University. Her research interests include channel coding, wireless communications, complex networks and chaos-based digital communications.



Francis C. M. Lau received the BEng(Hons) degree in electrical and electronic engineering and the PhD degree from King's College London, University of London, UK. He is the Associate Dean (Global Engagement) of the Faculty of Engineering and a Professor with the Department of Electrical and Electronic Engineering, The Hong Kong Polytechnic University, Hong Kong SAR. He is also a Fellow of IEEE and a Fellow of IET.

He is a co-author of two research monographs. He is also a co-holder of six US and four Chinese

patents. He has published more than 360 papers. His main research interests include channel coding, cooperative networks, wireless sensor networks, chaos-based digital communications, applications of complex-network theories, and wireless communications. He is a co-recipient of one Natural Science Award from the Guangdong Provincial Government, China; one Natural Science Award from the Chinese Institute of Electronics; eight best/outstanding conference paper awards; one technology transfer award; two young scientist awards from International Union of Radio Science; and one FPGA design competition award. He is among world's top 2% scientists in 2020, 2021 and 2022 according to the metrics compiled by Stanford University.

He was the General Co-chair of International Symposium on Turbo Codes & Iterative Information Processing (2018) and the Chair of Technical Committee on Nonlinear Circuits and Systems, IEEE Circuits and Systems Society (2012-13). He served as an associate editor for IEEE TRANSACTIONS ON CIRCUITS AND SYSTEMS II (2004-2005 and 2015-2019), IEEE TRANSACTIONS ON CIRCUITS AND SYSTEMS II (2006-2007), and IEEE CIRCUITS AND SYSTEMS MAGAZINE (2012-2015). He has been a guest associate editor of INTERNATIONAL JOURNAL AND BIFURCATION AND CHAOS since 2010.